UNIVERSITY OF ICELAND

FACULTY OF CIVIL AND ENVIRONMENTAL ENGINEERING
VR-II – Hjardarhagi 2-6, 107 Reykjavik, Iceland
Tel. +354 525 4700 · von.hi.is

**Manuscript published in 'Bulletin of Engineering Geology and the Environment'**

Olafsdottir, E.A., Erlingsson, S. & Bessason, B. (2023). Hybrid non-invasive characterization of soil strata at sites with and without embedded lava rock layers in the South Iceland Seismic Zone. *Bull Eng Geol Environ* 82, 146. https://doi.org/10.1007/s10064-023-03136-0

**Date of acceptance:**
23/02/23

**Title:**
Hybrid non-invasive characterization of soil strata at sites with and without embedded lava-rock layers in the South Iceland Seismic Zone

**Authors:**
Elin Asta Olafsdottir
Faculty of Civil and Environmental Engineering, University of Iceland, Reykjavik, Iceland
E-mail: elinasta@hi.is
ORCID: 0000-0002-9166-8406

Sigurdur Erlingsson
Faculty of Civil and Environmental Engineering, University of Iceland, Reykjavik, Iceland
Pavement Technology, Swedish National Road and Transport Research Institute, Linköping, Sweden
E-mail: sigger@hi.is
ORCID: 0000-0002-4256-3034

Bjarni Bessason
Faculty of Civil and Environmental Engineering, University of Iceland, Reykjavik, Iceland
E-mail: bb@hi.is
ORCID: 0000-0002-7963-0763

**Corresponding author:**
Elin Asta Olafsdottir
Faculty of Civil and Environmental Engineering, University of Iceland,
Hjardarhagi 2-6, IS-107 Reykjavik, Iceland
E-mail: elinasta@hi.is

**Hybrid non-invasive characterization of soil strata at sites with and without embedded lava-rock layers in the South Iceland Seismic Zone**

Elin Asta Olafsdottir, Sigurdur Erlingsson and Bjarni Bessason

## Abstract

The geological setting of Iceland is unusual, with highly jointed rock mass, loose sediments created in glacial outburst floods and eruptions, and layers of lava-rock embedded in or overlying soft sediments. This study aims to assess the feasibility of a composite analysis of dispersion and ellipticity curves for characterization of two of the primary classes of soil sites in the South Iceland Seismic Zone. Specifically, it seeks to develop a cost-effective workflow to identify and characterize sites where a layer of lava-rock is embedded in the sedimentary stratum at shallow depth, along with deep soil site characterization. Microtremor HVSR (horizontal-to-vertical spectral ratio) is found to be efficient to distinguish between sedimentary sites with and without an embedded lava-rock layer. The results further demonstrate the effectiveness of hybrid ellipticity and dispersion curve inversion to characterize soil sites with an embedded layer of lava-rock, which results in a strong velocity reversal with depth. Consistent with previous studies, the hybrid dispersion-ellipticity inversion is also found efficient for characterization of sites with a simpler structure.

## Keywords

Shear wave velocity; Surface wave analysis; Rayleigh wave ellipticity; Velocity reversal; Embedded lava-rock layers

## Acknowledgments

This work was supported by the Icelandic Research Fund (grant numbers 206793-053, 218149-051); the Icelandic Road and Coastal Administration; and the Energy Research Fund of the National Power Company of Iceland.

## Statements and Declarations

*Competing Interests*

The authors have no relevant financial or non-financial interests to disclose.

## 1. Introduction

Iceland is the largest island on the Mid-Atlantic Ridge, the divergent plate boundary between the Eurasian and North American tectonic plates. Across Iceland, the plate boundary is shifted towards east through two transform zones, the South Iceland Seismic Zone (SISZ) in the South Iceland Lowland, and the Tjörnes Fracture Zone (TFZ) in the north and off the northern coast (Einarsson 1991, 2008). The largest earthquakes in Iceland occur within the SISZ and TFZ, mostly associated with strike-slip motion at shallow depth (5–10 km) and have reached magnitudes of $M_w$ 7 (Einarsson 2008; Jónasson et al. 2021). The seismic hazard within these two zones is the highest in Northern Europe and comparable to that in Italy, Greece, Romania, and Turkey (Grünthal et al. 1999a, 1999b).

The SISZ crosses the largest and most populous agricultural region in Iceland. Destructive earthquakes in the SISZ tend to occur in sequences, typically every hundred years (Einarsson 2008). One such sequence began in 1896 when five $M_s \geq 6.0$ earthquakes struck the South Iceland Lowland over a two-week period. A sixth quake ($M_s$ 7.0), which many seismologists consider as the last event in the sequence, occurred in 1912. Since 2000, three major earthquakes have struck South Iceland. Two earthquakes of magnitude $M_w$ 6.5 and $M_w$ 6.4 occurred in June 2000, followed by an $M_w$ 6.3 event in May 2008 (Jónasson et al. 2021). The three events all inflicted structural damage in the region and caused landslides, rock fall, lateral spreading, and liquefaction, but no residential buildings collapsed and there was no loss of life (Skúlason et al. 2002; Sigbjörnsson et al. 2009; Vogfjörð et al. 2013; Bessason and Bjarnason 2016; Bessason et al. 2022).

The characteristics of Icelandic soil sites are, in many aspects, different from those in countries with a different geological history (Erlingsson 2019). The soil deposits in South Iceland are geologically young, of volcanic origin and have in many cases been formed in catastrophic events, including glacial outburst floods and ash fall from volcanic eruptions. Sites where one or more layers of igneous rock are sandwiched between soft sediments, or vice versa, are further common in the South Iceland Lowland. The geological structure is known to have a predominant effect on the characteristics of ground surface motion in the event of an earthquake and, consequently, on seismic loads and the nature of seismic induced damage. For sites in Iceland underlain by thick late-glacial and post-glacial sediments, the lack of information on the soil stiffness properties at depth has largely prevented detailed analytical studies on site response. At sites characterized by alternating layers of lava-rock and alluvial sediments, previous findings (Bessason and Kaynia 2002; Rahpeyma et al. 2016) have highlighted the significantly intensified ground motion as compared to rock sites. However, it can be challenging to identify such sites in practice, except by drilling sufficiently deep boreholes. Locations where a layer of lava-rock is embedded in soft sediments may, therefore, be misinterpreted as rock sites or as shallow sediments above bedrock. Furthermore, measurements of the shear wave velocity ($V_S$) profile of sandwiched lava-rock/soil structures in Iceland have not previously been conducted.

In the absence of site-specific analysis, present building codes (e.g., BSSC 2020; CEN 2004) use the time-averaged shear wave velocity in the top 30 m ($V_{S,30}$) as a proxy to account for the effects of the local soil conditions on the seismic action. Such simplified site characterization has, however, been found to misrepresent lava-rock/sedimentary soil structures (Bessason and Kaynia 2002; Rahpeyma et al. 2016; Sigurðsson et al. 2017). Moreover, it is uncertain that a site characterization based on the depth of the seismic bedrock formation and the corresponding time-averaged $V_S$, as proposed in the 2021-draft of Eurocode 8 (Paolucci et al. 2021), applies for such conditions. The overall site response is primarily controlled by the properties of the sediment layers and the average properties become less important. For evaluation of site-specific seismic loads, it is therefore essential to be able to identify and characterize sites with a sandwiched lava-rock/sedimentary structure in a time- and cost-effective way. In particular, the prospect of using non-invasive measurements for characterization of such sites is significant for seismic design of structures in geologically complex areas like Iceland.

Non-invasive geophysical techniques, including shallow seismic refraction (SSR), ground penetrating radar (GPR), electrical resistivity imaging (ERI), horizontal-to-vertical spectral ratio (HVSR, H/V) and surface wave measurements (SWM), are widely used to delineate the subsurface structure and assess soil parameters (e.g., Steeples 2005; Kramer 2014). Applications include seismic site characterization and assessment of site-effect proxies (e.g., Castellaro and Mulargia 2009; Akın and Sayıl 2016; Assaf et al. 2022), identification of groundwater levels (e.g., Grelle and Guadagno 2009; Sharafeldin et al. 2019), and evaluation of rock quality (e.g., Hasan and Shang 2022). Active- and passive-source methods have also been employed to identify near-surface low-velocity zones (Ivanov et al. 2006; Wang et al. 2022) and low-velocity anomalies at greater depth (Sarjan et al. 2021). SWM, in conjunction with analysis of Rayleigh wave ellipticity, have further been applied to identify stiff inclusion layers and associated low-velocity zones using both real-world (Michel et al. 2014) and synthetic data (Hallo et al. 2021). However, in the Icelandic geological setting, the use of non-invasive geophysical measurements to detect the depth and thickness of relatively thin layers of lava-rock imbedded in soft sediments is a previously unexplored topic.

For sedimentary sites in the South Iceland Lowland, SWM have been found to be well-suited for evaluation of soil $V_S$ profiles (e.g., Bessason et al. 1998; Bessason and Erlingsson 2011; Olafsdottir et al. 2019; Erlingsson et al. 2022). However, the depth retrieved in active-source surveys (e.g., MASW, Park et al. (1999)) is often insufficient for adequate evaluation of site response and the depth of the seismic bedrock formation is not constrained. Microtremor array measurements (MAM) were recently conducted for the first time in South Iceland (Olafsdottir et al. 2022) to extend active-source dispersion curves to lower frequencies and, hence, increase the prospective investigation depth at deep alluvial sedimentary sites. However, several different aperture arrays are usually required to retrieve the $V_S$ profile down to a depth of several tens to a few hundreds of meters (Foti et al. 2018), making the data acquisition time-consuming. Furthermore, space constraints in urban areas or geological restrains, e.g., lateral variations in soil properties or layering, can hinder the use of large-aperture arrays.

Without additional information on the geological structure, MASW and MAM measurements have been found to be insufficient to identify and characterize sites with alternating layers of soft sediments and lava-rock in the SISZ. The single-station HVSR technique has previously been applied at selected locations in South Iceland for analysis of both microtremors and strong-motion data (Atakan et al. 1997; Bessason and Kaynia 2002; Olivera et al. 2014; Halldorsson et al. 2016; Rahpeyma et al. 2016; Sigurðsson et al. 2017; Olafsdottir et al. 2022). This includes sites with alternating layers of soft sediments and lava-rock, where the predominant frequency/frequencies of the retrieved HVSR curves have been modelled using equivalent linear analysis in SHAKE (Bessason and Kaynia 2002) and dynamic response theory of a classically damped linear oscillator subjected to a base excitation (Rahpeyma et al. 2016). The layer structures were in both studies supported by geological mapping and data from geotechnical boreholes. Forward computation of the HVSR requires a-priori assumptions on the contribution of different types of waves to the recorded wavefield (e.g., Endrun 2011; Hobiger et al. 2013). By identifying the Rayleigh wave ellipticity, i.e., the ratio between the horizontal and vertical axes of the elliptical particle motion of Rayleigh waves, (Hobiger et al. 2009, 2013) and specifying the experimental ellipticity curve as an inversion target, the need for estimating the effects of other wave types in the forward modelling is avoided. Inversion of HVSR or Rayleigh wave ellipticity curves alone can provide an ambiguous estimate of the soil stiffness properties, as the ellipticity only constrains the shape of the velocity profile but not the absolute values of the seismic wave velocities and the depth of the layer interfaces (Scherbaum et al. 2003; Hobiger et al. 2013). Prior studies have, however, indicated that inverting dispersion curves with complementary information extracted from single-station measurements can extend the investigation depth of SWM, provide better constrained estimates of layer interfaces, facilitate dispersion curve mode identification and, ultimately, aid the selection of realistic $V_S$ models (e.g., Scherbaum et al. 2003; Arai and Tokimatsu 2005; Parolai et al. 2005; Picozzi et al.

2005; Boaga et al. 2013; Hobiger et al. 2013; Michel et al. 2014; Gouveia et al. 2018). Such joint analysis has not previously been attempted for Icelandic geological structures.

The aim of this study is to assess the feasibility of a composite inversion of dispersion and ellipticity curves for seismic site characterization of both simple and complex soil structures in the South Iceland Seismic Zone. Particularly, this work describes a cost-effective workflow to identify and characterize sites where a relatively thin layer of lava-rock is embedded in the soft sedimentary stratum. For this purpose, microtremor single-station measurements and active- and passive-source surface wave analysis (MASW, MAM) were conducted at four infrastructure sites in South Iceland. The sites, referred to as Landeyjar Harbor, Markarfljót Bridge, Stóra-Laxá Bridge and Óseyri Bridge (Fig. 1), were selected because of their importance for the Icelandic transport network. They are further divided into two groups based on their geological setting and are considered to represent two of the primary classes of soil sites in the South Iceland Lowland. The Landeyjar Harbor and Markarfljót Bridge sites are characterized by thick alluvial sediments consisting of sand and sandy gravel. At the Stóra-Laxá Bridge and Óseyri Bridge sites, a layer of lava-rock is sandwiched between sedimentary layers within the top 10–20 m. Hence, this study offers important insights into the site characteristics of two of the most common soil site structures in the South Iceland Seismic Zone. The results are compared with geological information and available borehole data.

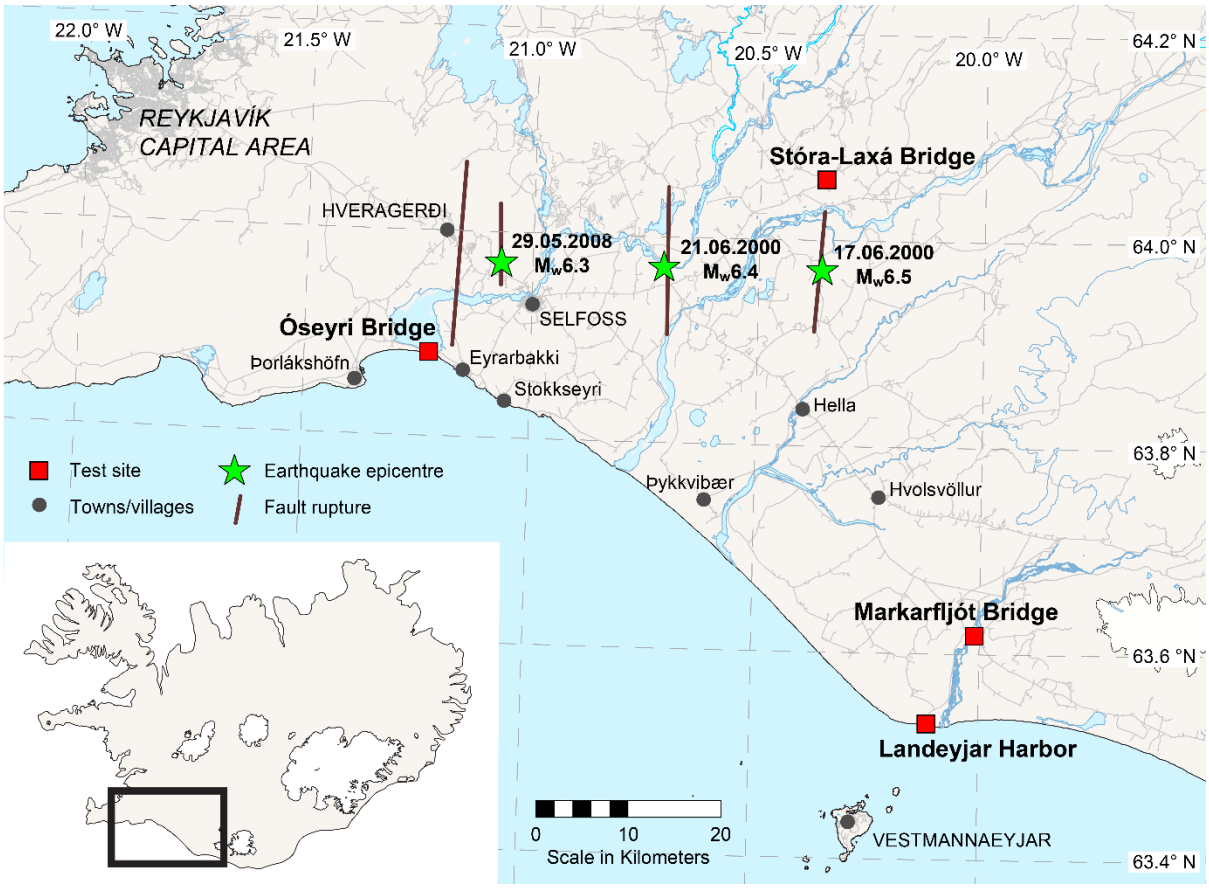


***Fig. 1*** *Epicenters and fault ruptures of the June 2000 South Iceland earthquakes and the May 2008 Ölfus earthquake. Locations of the four research sites in this work, Landeyjar Harbor, Markarfljót Bridge, Stóra-Laxá Bridge and Óseyri Bridge (red squares). [The map contains data (IS 50V) from the National Land Survey of Iceland from 12/2020. Earthquake magnitudes and epicenters are from the ICEL-NMAR Earthquake Catalog (Jónasson et al. 2021)]*

## 2. Research sites and geological setting

The geology of the South Iceland Lowland results from a combination of volcanic activity, glacial drift, and changes in sea level through the ages (Sæmundsson 1979; Atakan et al. 1997; Bessason and Kaynia 2002; Sigbjörnsson and Ólafsson 2004; Erlingsson 2019). Iceland was covered by a glacier plateau during the last glaciation period and the South Iceland Lowland was partially a seabed. As the glacier retreated and the land rose, thick layers of fluvial, glacial, and glacio-fluvial sediments were built up in South Iceland. Post-glacial sedimentary layers, resulting from repeated glacial outburst floods and the deposition of volcanic materials during eruptions, are common along the coastline and close to main riverbeds. The soil deposits are primarily characterized by coarse-grained aggregates, i.e., coarse silty particles, sand, and courser grains, and, due to the rapid sediment build-up, they are often loosely compacted (Erlingsson 2019). In many areas in the South Iceland Lowland, the sedimentary layers have been covered by layers of basaltic lava and hyaloclastite breccia from the post-glacial period (Atakan et al. 1997; Bessason and Kaynia 2002; Sigbjörnsson and Ólafsson 2004; Rahpeyma et al. 2016), thus, creating soil structures with layers of lava-rock on top of, or embedded in, unconsolidated sediments. The thickness of the lava-rock may be up to 10 m, whilst the sediments can be much thicker (Einarsson 1994, Sigbjörnsson and Ólafsson 2004). Such alternation of soft sedimentary layers and stiff lava-rock creates strong velocity reversals with depth. The presence of tectonic factures, fissures and faults further adds to the complexity of the surface geology in South Iceland (Clifton and Einarsson 2005; Einarsson 2010).

The first site considered in this work is by the Landeyjar Harbor on the South Iceland coast. Landeyjar Harbor is a ferry sea portal, constructed between 2008 and 2010, which connects the mainland of Iceland and the Vestmannaeyjar archipelago. The Landeyjar Harbor area is characterized by thick sediments of littoral black basalt sand and sandy gravel. The total sediment thickness is unknown. The depth to the groundwater level in the area has been estimated to be in the range of 3–5 m in prior studies (Bessason and Erlingsson 2011; Olafsdottir et al. 2019). In modern times, the area surrounding the harbor has experienced significant sand transport. The glacial Markarfljót River is located around 2.5 km east of the harbor area and discharges an estimated 100,000–200,000 $m^3$ of sand to the coastal zone annually (Pétursson et al. 2020). The river is highly dynamic and prior studies have indicated that the river mount migrates in a cyclical pattern along a few kilometer wide part of the coastline (Viggosson et al. 2005). Furthermore, glacial outburst floods have repeatedly occurred in Markarfljót River (Larsen et al. 2005), e.g., due to volcanic eruptions underneath Mýrdalsjökull Glacier, which historically have reached an estimated discharge of 150,000–250,000 $m^3/s$ (Gröndal et al. 2005) and transported enormous amounts of soil materials. For comparison, the Eyjafjallajökull eruption in 2010 "only" caused a peak discharge of 560 $m^3/s$ in Markarfljót River. Nevertheless, it was necessary to emergently divert the river to save the bridge (Larsen et al. 2013).

The second site is located by the abovementioned Markarfljót Bridge, which is a 250 m long steel beam bridge approximately 11 km north-east of Landeyjar Harbor. The soil deposits by Markarfljót Bridge are primarily characterized by thick sediments of sandy gravel, which are expected to have primarily been created in outburst events. The estimated groundwater level is at a depth of 2–4 m. A shallow borehole, located 95 m south-east of the test site, indicates layers of loose and more densely compacted sand and gravel down to a depth of 17.7 m. Below that, the borehole log identifies a stiffer layer of unknown thickness, possibly comprised of partly cemented sediments. The borehole was terminated at a depth of 19.7 m before reaching bedrock. Hence, the depth to bedrock is unknown but based on the geological history of the area it is expected to be somewhat shallower than in the Landeyjar Harbor area.

The third test site is located by the Stóra-Laxá River, approximately 3 km north of the fault rupture of the June 17, 2000 South Iceland Earthquake. Strong-motion records are not available for the Stóra-Laxá site (Bessason et al. 2019). A bridge was constructed at the site in 1983. It is a 120 m long three-span

base-isolated RC single-lane beam bridge, oriented in a NE-SW direction. The bridge was open for traffic immediately after the June 17, 2000, earthquake, however, there was post-earthquake evidence that its superstructure had moved by ±5 cm as pounding of the superstructure and the abutments was observed (Bessason et al. 2019). In 2023, a new 145 m long four-span RC base-isolated beam bridge is being constructed next to the old bridge. Geotechnical borings conducted at the site indicate a sandwiched soft-stiff-soft stratigraphy on both sides of the river. On the north-eastern side, where the measurements in this study were conducted, borehole data (Fig. 2) shows that the surficial soil cover has a thickness of 0.5–1 m and rests on a c.a. 5 m thick layer of medium to dense gravel. Between depths of 5.5–6 m and 11–13 m is a layer of scoria, i.e., highly vesicular igneous rock. Below the scoria are thin layers comprised of silt, sand and/or gravel. The borings were terminated at a depth between 13.8 m and 23.7 m before reaching bedrock. No data is available for depths exceeding 23.7 m. The borehole locations (T-12, T-13, T-15, and T-16) are shown relative to the surface wave arrays at the Stóra-Laxá site in Fig. 4c.

The fourth test site is located by the western abutment of the Óseyri Bridge. The Óseyri Bridge was constructed in 1988 and is a 370 m long base-isolated, continuous post-tensioned two-beam concrete bridge, built in eight spans with two abutments and seven concrete piers (Bessason et al. 2019). It is located at the estuary of the Ölfusá River, less than 2 km from the southern end of the main fault rupture of the May 2008 $M_w$ 6.3 Ölfus Earthquake. The bridge was exposed to severe earthquake loads, most likely including a strong near-fault pulse, but only suffered minor damage (Jonsson et al. 2010; Bessason et al. 2019). No strong-motion records are available for the bridge site. The surficial soil layers by the Óseyri Bridge are characterized by loose black basalt silty sand. The exact thickness of the sediments is unknown. However, the abutments and piers of the Óseyri Bridge are founded on fractured rock at a depth of 9.5 m below the bridge deck (Icelandic Road Administration 1986), corresponding to a depth of around 5.5 m below surface level. This may suggest a comparable depth to a stiff layer at the surveyed site. Borings conducted on the eastern bank of the river, approximately 350 m from the eastern abutment, indicate the presence of a second sand layer below the fractured lava-rock. However, based on available data, the depth and thickness of the presumed lava-rock layer is not constrained.

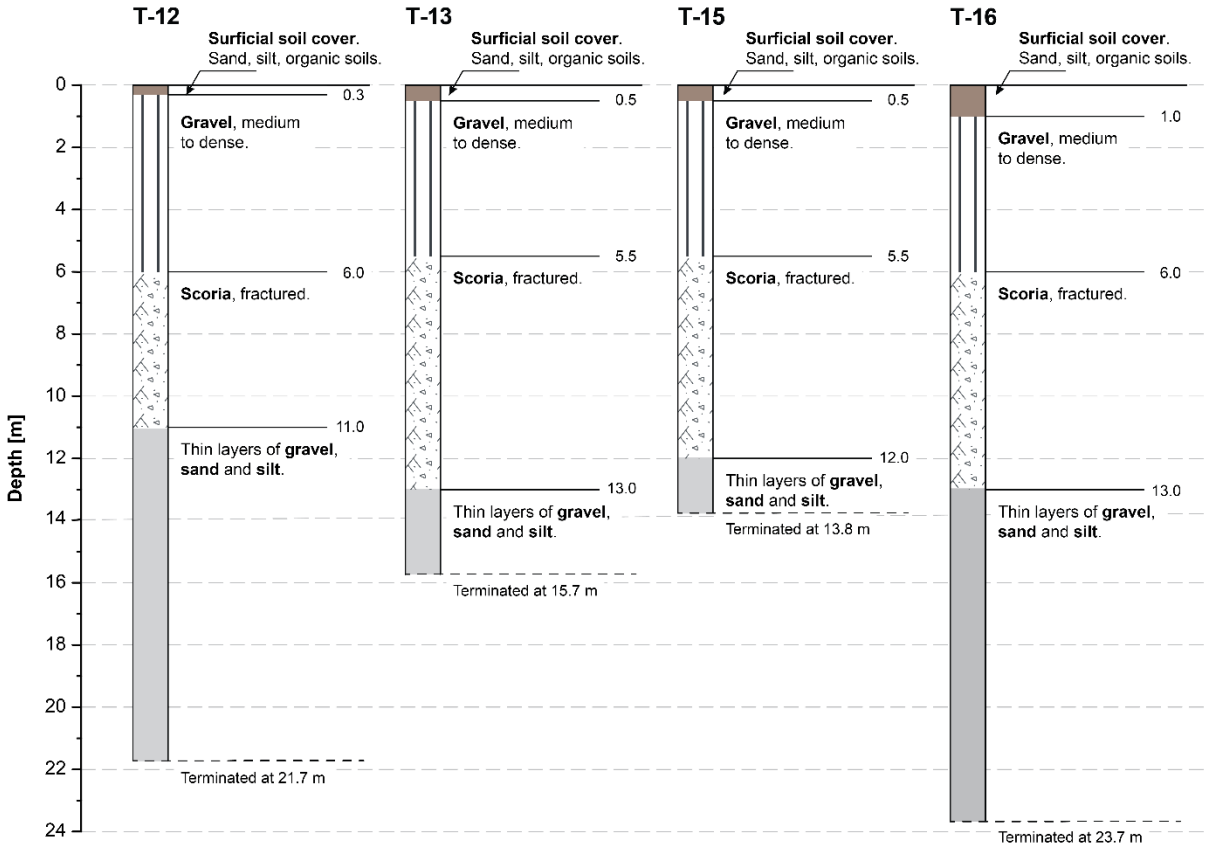


***Fig. 2*** *Stratigraphy of the Stóra-Laxá Bridge site based on geotechnical borings conducted at the site. The borings were terminated at a depth between 13.8 m and 23.7 m before reaching bedrock*

## 3. Data acquisition and processing

### *3.1 Data acquisition*

The active-source (MASW) time series were collected using twenty-four vertical 4.5 Hz geophones (GS-11D from Geospace Technologies), arranged in a linear array with equal receiver spacing $dx$. The geophones were connected to two data acquisition cards (NI USB-6218 from National Instruments) and a computer equipped with customized multi-channel DAQ software (Olafsdottir 2019). At each site, two or three MASW arrays with a common midpoint and orientation but different $dx$ (in the range of 0.5–2 m) were used for data acquisition (Fig. 3). The impact load was created by a 6.3 kg sledgehammer that was struck on a 15 cm-diameter metallic base plate, in-line with the receivers, at several different offsets from both ends of each array. Repeated shots were collected for each profile length and source location. The sampling rate was 1000 Hz and the total recording duration for each shot was 2.2 s (including a 0.2 s pre-trigger). The longest MASW array used at each site is shown in Fig. 4. At the Stóra-Laxá site, the receiver arrays were placed parallel to the existing boreholes. At the Landeyjar Harbor, Markarfljót Bridge and Óseyri Bridge sites, the arrays were positioned close to the respective structures, while avoiding natural surface reliefs and road embankments. As the primary aim of the current study is to assess the feasibility of the hybrid analysis for characterization of these two primary classes of soil sites, a single test location at each site was considered sufficient.

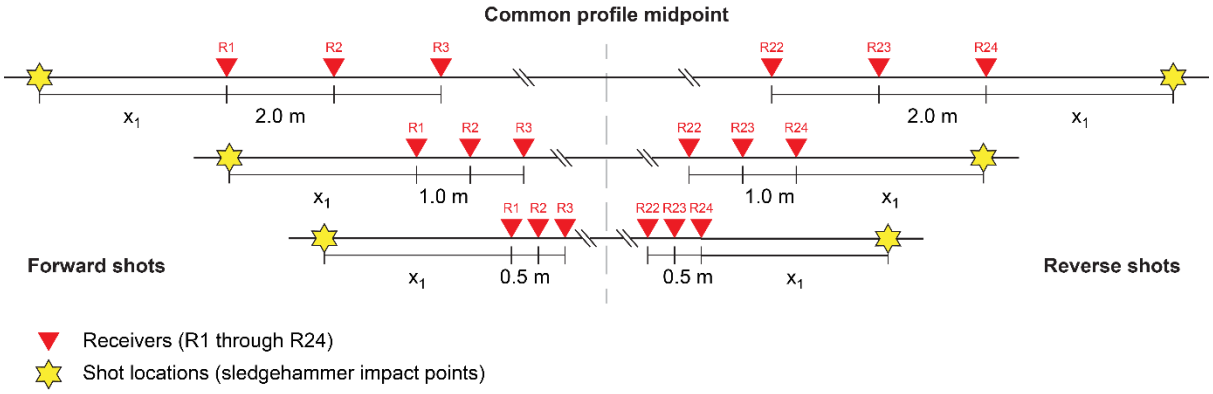


***Fig. 3*** *Geometry of MASW receiver arrays. Each array consists of 24 vertical geophones lined up with equal receiver spacing. The receiver spacing was changed while keeping the midpoint and orientation of the array fixed. The source offset length ($x_1$) is given in Table 1 for each of the four sites*

The passive-source data acquisition was conducted using a set of four broadband three-component Lennartz 5 s seismometers, each coupled to a Reftek 130-01 digitizer. The seismometers were arranged in equilateral triangular-shaped arrays (Fig. 4) with a circumradius in the range of 6–24 m. At the Landeyjar Harbor, Markarfljót Bridge and Óseyri Bridge sites, respectively, the centroid of the nested triangles corresponded to the midpoint of the active-source (MASW) receiver arrays. Due to logistical constraints at the Stóra-Laxá site, the centroid of the triangular array was located a few meters north-west of the midpoint of the MASW array (Fig. 4c). The acquired ambient vibrations were sampled at a frequency of 200 Hz with a continuous GPS synchronization. The recording duration at each site was 50–60 min and conducted under favorable weather conditions, i.e., no rain and low wind. The active and passive array geometries are summarized in Table 1.

***Table 1*** *Overview of the active- and passive-source surface wave datasets acquired at the Landeyjar Harbor, Markarfljót Bridge, Stóra-Laxá Bridge and Óseyri Bridge sites*

| Site | Dataset | No. channels | Array layout | Recording time |
|---|---|---|---|---|
| **Landeyjar Harbor** | Active | 24 | Linear, $dx$ = 0.5 m<br>- Forward: $x_1$ = 3, 5, 7.5 m<br>- Reverse: $x_1$ = 3, 5 m | $T$ = 2.2 s |
| | | | Linear, $dx$ = 1.0 m<br>- Forward: $x_1$ = 5, 7.5, 10, 15, 20 m<br>- Reverse: $x_1$ = 5, 10, 15 m | $T$ = 2.2 s |
| | | | Linear, $dx$ = 2.0 m<br>- Forward: $x_1$ = 5, 7.5, 10, 15, 20, 25 m<br>- Reverse: $x_1$ = 5, 10, 15 m | $T$ = 2.2 s |
| | Passive | 4 | Triangular, $r$ = 12 m | $T$ = 60 min |
| | | | Triangular, $r$ = 24 m | $T$ = 60 min |
| **Markarfljót Bridge** | Active | 24 | Linear, $dx$ = 1.0 m<br>- Forward: $x_1$ = 5, 7.5, 10, 15, 20 m<br>- Reverse: $x_1$ = 5, 10, 15 m | $T$ = 2.2 s |
| | | | Linear, $dx$ = 2.0 m<br>- Forward: $x_1$ = 5, 7.5, 10, 15, 20, 25 m<br>- Reverse: $x_1$ = 5, 10 m | $T$ = 2.2 s |
| | Passive | 4 | Triangular, $r$ = 12 m | $T$ = 60 min |
| | | | Triangular, $r$ = 24 m | $T$ = 60 min |
| **Stóra-Laxá Bridge** | Active | 24 | Linear, $dx$ = 0.5 m<br>- Forward: $x_1$ = 3, 5, 7.5, 10, 12.5 m | $T$ = 2.2 s |

| | | | | |
|---|---|---|---|---|
| | | | - Reverse: $x_1$ = 10 m | |
| | | | Linear, $dx$ = 1.0 m<br>- Forward: $x_1$ = 5, 7.5, 10, 15, 20 m<br>- Reverse: $x_1$ = 5, 10, 15 m | $T$ = 2.2 s |
| | Passive | 4 | Triangular, $r$ = 6 m | $T$ = 60 min |
| **Óseyri Bridge** | Active | 24 | Linear, $dx$ = 1.0 m<br>- Forward: $x_1$ = 5, 7.5, 10, 15, 20 m<br>- Reverse: $x_1$ = 5, 10, 15 m | $T$ = 2.2 s |
| | | | Linear, $dx$ = 2.0 m<br>- Forward: $x_1$ = 5, 7.5, 10, 15, 20, 25, 30 m | $T$ = 2.2 s |
| | Passive | 4 | Triangular, $r$ = 6 m | $T$ = 50 min |
| | | | Triangular, $r$ = 12 m | $T$ = 60 min |
| | | | Triangular, $r$ = 24 m | $T$ = 50 min |

$dx$: Receiver spacing. $x_1$: Source offset length. $r$: Circumradius. $T$: Total recording time.

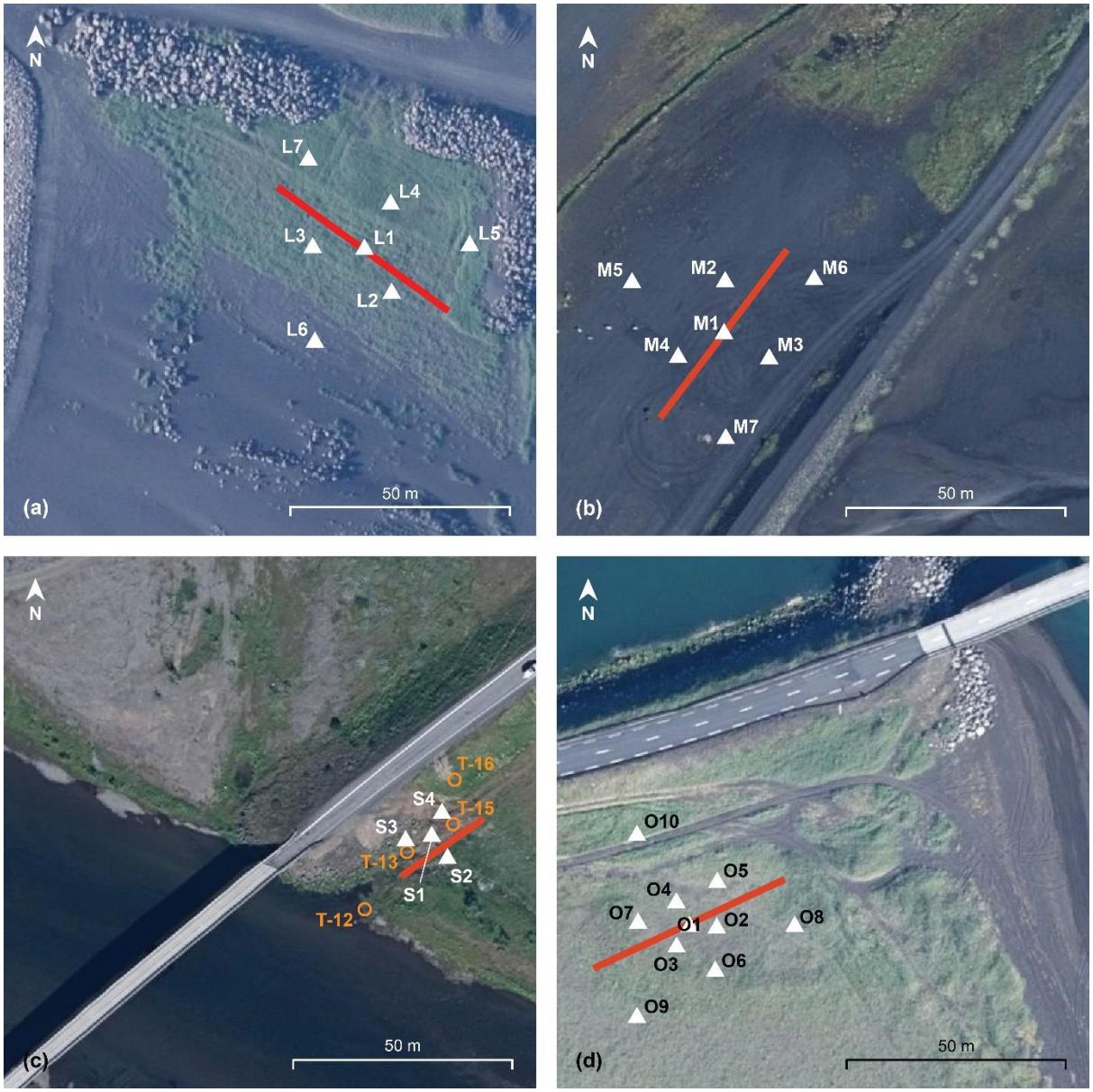


***Fig. 4*** *Aerial view of the* ***a*** *Landeyjar Harbor,* ***b*** *Markarfljót Bridge,* ***c*** *Stóra-Laxá Bridge and* ***d*** *Óseyri Bridge sites. The red lines show the longest active-source (MASW) survey profile at each of the sites. Seismometer positions are shown by white triangles and labelled as L1-L7 (Landeyjar Harbor), M1-M7 (Markarfljót Bridge), S1-S4 (Stóra-Laxá Bridge) and O1-O10 (Óseyri Bridge). The locations of the geotechnical borings (T-12, T-13, T-15, and T-16) conducted at the Stóra-Laxá site are shown by orange circles. [Areal images are from the database of the National Land Survey of Iceland.]*

*3.2 Microtremor horizontal-to-vertical spectral ratio*

The HVSR method is based on computation of the spectral ratio between the horizontal and vertical components of surface ground motion (Nakamura 1989; SESAME 2004; Molnar et al. 2022). It is well-recognized that the shape of the HVSR amplification curve is strongly related to the local subsoil structure. For instance, a single well-defined peak is indicative of a large impedance contrast which results in an amplification of the horizontal ground motion relative to its vertical component. The predominant frequency of the soil deposits may then be approximated as the frequency of the HVSR peak value. For the simple case of an 1D soil model consisting of a uniform soft sedimentary layer above bedrock, the resonance frequency of the $n$-th mode ($f_n$) can be theoretically estimated as (Kramer 2014)

$$f_n = \frac{V_S}{4H}(2n+1) \quad \text{for} \quad n = 0, 1, 2, \ldots \tag{1}$$

where $H$ is the layer thickness, $V_S$ is the layer shear wave velocity and $n$ is the mode number.

The microtremor HVSR for each measurement station was obtained in accordance with the recommendations of SESAME (2004). The recorded three-component ambient vibrations were split into 50 s windows. The Fourier amplitude spectrum of each component was computed over the window duration and smoothed using the Konno-Ohmachi function (Konno and Ohmachi 1998) with a filter coefficient of $b = 40$. The HVSR of each time window was subsequently obtained by dividing the geometric mean of the two smoothed horizontal spectra by the spectrum for the vertical component.

*3.3 Rayleigh wave ellipticity curves*

Two single-station techniques were used to evaluate the Rayleigh wave ellipticity as a function of frequency for the respective sites, RayDec and HVTFA (H/V using time-frequency analysis).

The RayDec method, proposed by Hobiger et al. (2009) and further described by Hobiger et al. (2013), is based on the random decrement technique (Asmussen 1997). The two free parameters of the method, the time window length ($\Delta$) and the bandwidth used in filtering the data ($df$), were set equal to their suggested values as $\Delta = 10/f$ and $df = 0.1f$, where $f$ is the frequency of interest. To assess the ellipticity for a given measurement station, the recorded microtremors were split into six 8–10 min segments, depending on the total signal length, that were processed separately. The median ellipticity curve for the respective station was then obtained by assuming the lognormal distribution for the estimated ellipticity values at each frequency.

The HVTFA analysis was conducted using the HVTFA module in the Geopsy software package (Wathelet et al. 2020). A description of the HVTFA module workflow and its mathematical principles is provided in Fäh et al. (2009). The two free parameters of the HVTFA technique, the Morlet wavelet parameter ($m$) and $nppm$, the number of maxima in the vertical component used per minute, were specified as $m = 8$ and $nppm = 3$, which is in line with the recommendations provided in Fäh et al. (2009). Although not shown, the recorded microtremors were reprocessed with different values of $nppm$ in the suggested range of 1–5 maxima per minute, which provided comparable lognormal median ellipticity curves. Low values of $nppm$, e.g., $nppm = 1$, theoretically restrict the computation of the H/V ratio to the most energetic Rayleigh waves in the signal. However, due to the relatively short recording time (Table 1), a slightly higher value of $nppm$ was selected to obtain a better estimate of the lognormal median ellipticity curve and its associated standard deviation.

*3.4 Rayleigh wave dispersion curves*

The experimental dispersion curves were retrieved by a combination of active- and passive-source SWM. The active-source time series were analyzed using the phase shift method (Park et al. 1998) as implemented in the dispersion analysis tool of the MASWaves software (Olafsdottir et al. 2018b). Each multi-channel record was processed independently to obtain a statistical sample of dispersion curves and allow for analysis of the stability of the dispersion curve estimates.

The passive-source data was processed with the spatial autocorrelation method (Aki 1957; Bettig et al. 2001) using the MSPAC toolbox included in Geopsy (Wathelet et al. 2020). To quantify the variability in the estimated phase velocity values with frequency, the microtremors recorded by each triangular array were split into four 12.5–15 min sub-records, which were analyzed separately. Resulting from the data acquisition layout, the possible combinations of receiver pairs for each array were arranged in two rings, each consisting of three pairs. The spatial autocorrelation (SPAC) coefficients for each ring were computed by dividing the vertical components of the recorded microtremors into time-windows of length $100T$, where $T$ is the central period of each analyzed frequency band, with 10% overlap between windows. The dispersion curve corresponding to the given sub-record was subsequently derived from the retrieved SPAC curves and checked for consistency against a dispersion curve obtained using the same procedure on the entire 50–60 min record.

The active- and passive-source data was merged into a single broadband dispersion curve using an adapted version of the method outlined in Olafsdottir et al. (2018a) with the dispersion curve data points added up within logarithmically spaced frequency bands. The arithmetic mean and standard deviation of the phase velocity values within each band are subsequently used to construct the composite dispersion curve with upper and lower boundaries.

## 4. Experimental HVSR, ellipticity and dispersion curves

*4.1 Microtremor horizontal-to-vertical spectral ratio*

Figure 5 compares the lognormal median HVSR curves for each station of the triangular array formations at Landeyjar Harbor, Markarfljót Bridge, Stóra-Laxá Bridge and Óseyri Bridge. Also shown are the mean frequency of the first HVSR peak ($f_{0,HV}$) and the associated standard deviation ($\sigma_{f0,HV}$). For evaluation of $f_{0,HV}$ and $\sigma_{f0,HV}$, stations whose HVSR did not fulfil the clarity criteria specified in SESAME (2004) were omitted as they are considered less reliable for evaluation of $f_{0,HV}$. Where applicable, the mean and standard deviation of the frequency of the second peak ($f_{1,HV}$ and $\sigma_{f1,HV}$) were obtained in the same manner, with the SESAME criteria applied to each peak separately.

The HVSR results for Landeyjar Harbor (Fig. 5a) and Markarfljót Bridge (Fig. 5b) show primarily unimodal amplification curves and provide an estimate of the predominant frequency of the respective sites as 0.62 ± 0.06 Hz (Landeyjar Harbor) and 0.88 ± 0.08 Hz (Markarfljót Bridge). The HVSR curves for Markarfljót Bridge further show a small broad peak at 4.39 ± 0.84 Hz which is likely related to the increase in stiffness detected at 15–20 m depth. Bimodal HVSR is retrieved for the Stóra-Laxá Bridge site with estimated peak frequencies of 2.83 ± 0.33 Hz and 9.32 ± 0.88 Hz (Fig. 5c), though displaying more inter-station variability than is observed at the other three sites. Based on the inferred soil stratigraphy by the Stóra-Laxá Bridge (Fig. 2), the second peak is presumably caused by the impedance contrast between the gravel sediments and the lava-rock layer. The HVSR curves retrieved by the western abutment of the Óseyri Bridge also display two peaks, one at a frequency of 1.14 ± 0.07 Hz and a second at 6.60 ± 0.75 Hz (Fig. 5d). In accordance with known geological features in the South Iceland Lowland, as well as similarity to observed HVSR at sites with embedded layers of lava-rock or scoria, the second peak is considered to indicate a stiff layer sandwiched between layers of soft sediments. Hence, the results shown in Fig. 5 support that the selected sites can be divided into two

groups based on soil stratigraphy, subsequently referred to as sedimentary sites (Landeyjar Harbor and Markarfljót Bridge) and sedimentary/lava-rock sites (Stóra-Laxá Bridge and Óseyri Bridge).

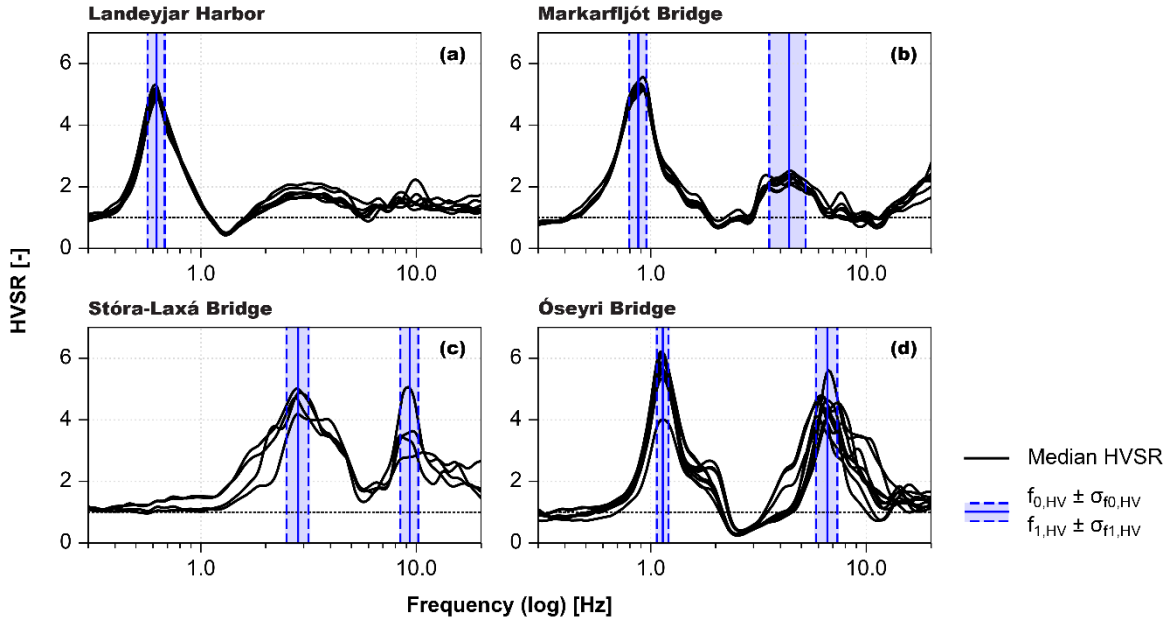


***Fig. 5*** *Lognormal median HVSR curves obtained for individual stations of the triangular array formations at* ***a*** *Landeyjar Harbor (7 stations),* ***b*** *Markarfljót Bridge (7 stations),* ***c*** *Stóra-Laxá Bridge (4 stations) and* ***d*** *Óseyri Bridge (10 stations). For enhanced clarity, standard deviation HVSR curves are not shown. The vertical lines represent the mean frequency of the HVSR peak(s) for each site and the associated plus/minus one standard deviation ($f_{0,HV} \pm \sigma_{f0,HV}$ for the first peak and, where applicable, $f_{1,HV} \pm \sigma_{f1,HV}$ for the second peak)*

### *4.2 Rayleigh wave ellipticity curves*

Figure 6 shows the ellipticity curves for each station of the triangular array formations at the four test sites. The ellipticity curves for the two sedimentary sites (Figs. 6ab), show single peaks that are clearly identified by both analysis techniques. The ellipticity retrieved for the different stations is consistent over the entire frequency range, particularly below 1.5–2 Hz, which is the frequency band of primary interest to constrain the depth to bedrock at both sites. The broad second peak observed in the HVSR results for the Markarfljót Bridge is further adequately retrieved by both techniques. The ellipticity curves for the central stations of the triangular arrays are compared to the corresponding HVSR in Figs. 7ab. The upper and lower boundary curves also shown correspond to plus/minus one standard deviation of the computed ellipticity or HVSR values. For both sites, the retrieved ellipticity is close to the computed HVSR, suggesting that the recorded wavefield is primarily composed of Rayleigh waves. However, the computed standard deviations differ substantially between methods. The RayDec analysis is conducted by splitting the recorded microtremors into 8–10 min windows, which show limited variability. This is consistent with the temporal consistency of RayDec analysis reported by Hobiger et al. (2009). The HVTFA standard deviations, however, result from statistical analysis of amplitude ratios identified by maxima on the vertical component of the recorded microtremors, which indicates significantly more variability in the computed ellipticity values.

The ellipticity results for each station at the two sedimentary/lava-rock sites are shown in Figs. 6cd. The RayDec and HVTFA analysis results indicate bimodal curves with peak frequencies consistent with

those retrieved by HVSR (Figs. 5cd). For Óseyri Bridge (Fig. 6d), the first ellipticity peak between 1.1 Hz and 1.2 Hz and the trough around 2.4 Hz are well constrained by both techniques. The two analysis techniques and the different stations provide more varied results for the second peak, notably its right flank. The estimated ellipticity for four stations (O1, O7, O8 and O9) indicates the presence of a smaller third peak around 9–10 Hz, or a broader peak in the higher-frequency range. Available information on the geological structure at the site is insufficient to conclude on the nature of the third or broad peak. It is, therefore, unknown if this results from multiple strong $V_S$ impedance contrasts in the local shallow ground structure, higher-mode interference, or other disturbances. It is, however, worth noting that the measurement stations where this is observed are not confined to a specific part of the testing area. This is therefore more likely a result of local disturbances than irregularities in the geological structure. Hence, the retrieved ellipticity for station O4, which is located adjacent to the MASW arrays at the site (Fig. 4d) and is free of this effect, was selected for further analysis. Characterization of multi-peak ellipticity curves retrieved at lava-rock sites with a more complex structure is outside the scope of this work. Furthermore, both analysis techniques yield ellipticity curves for station O4 that are in excellent agreement over the entire analyzed frequency range (Fig. 7d), which supports the reliability of the ellipticity data for this station. The RayDec and HVTFA ellipticity curves for Stóra-Laxá Bridge (Fig. 6c) are in reasonable agreement. In particular, the right flank of the first peak and the peak frequency are consistently retrieved by both techniques. The RayDec analysis tends though to indicate higher absolute amplitude for the ellipticity peak. This may, however, be related to a well-known problem associated with ellipticity assessment techniques (Hobiger et al. 2012, 2013), which encounter difficulties at the peak and trough frequencies where either the vertical or the horizontal component of the ellipticity ratio theoretically vanishes. The ellipticity curves for station S2 (Fig. 4c), which are used in the subsequent inversion analysis, are compared to the HVSR results for the same station in Fig. 7c.

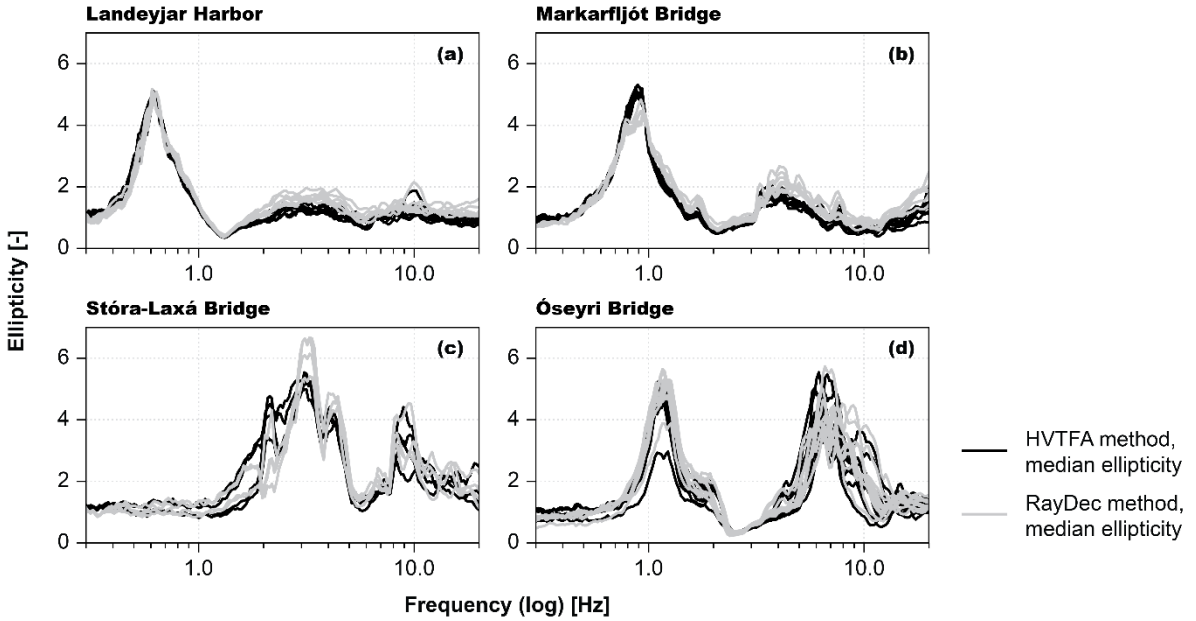


***Fig. 6*** *Lognormal median Rayleigh wave ellipticity curves obtained for individual stations of the triangular array formations at* ***a*** *Landeyjar Harbor,* ***b*** *Markarfljót Bridge,* ***c*** *Stóra-Laxá Bridge and* ***d*** *Óseyri Bridge. Two techniques were used to estimate the ellipticity curve for each station, HVTFA (black lines) and RayDec (gray lines)*

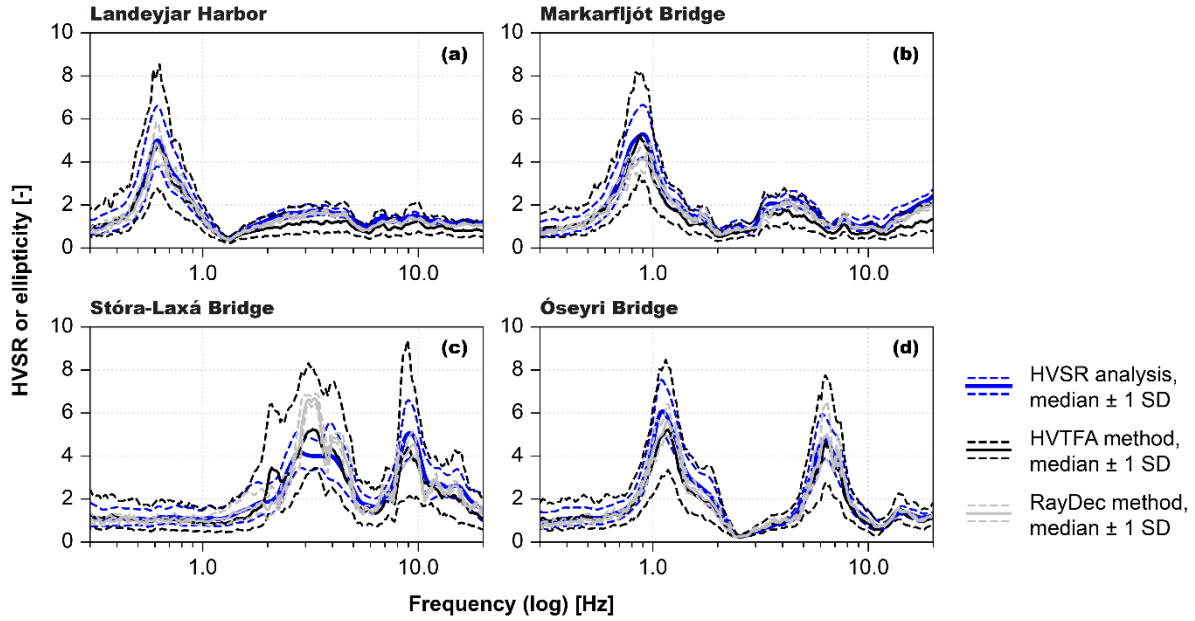


***Fig. 7*** *Lognormal median HVSR and Rayleigh wave ellipticity curves for the stations at* ***a*** *Landeyjar Harbor,* ***b*** *Markarfljót Bridge,* ***c*** *Stóra-Laxá Bridge and* ***d*** *Óseyri Bridge that were used in the composite dispersion and ellipticity curve inversions. The dashed lines represent the lognormal median plus/minus one standard deviation (SD) curves for each station*

*4.3 Rayleigh wave dispersion curves*

The identified active-source dispersion curves for the four sites are shown in Figs. 8a–d. Analysis of shots applied at different ends of the receiver arrays (referred to as 'forward' and 'reverse' measurements in Fig. 8) revealed in all cases very similar dispersion characteristics, thereby not indicating any significant lateral variations in material properties or soil stratigraphy at shallow depth beneath the respective receiver arrays. This observation is further supported by the low inter-station variability of the retrieved HVSR and ellipticity curves for each of the four sites (Figs. 5, 6). Therefore, a single orientation of the active-source survey profile is considered sufficient for subsequent analysis. The passive-source dispersion curve estimates for each site are shown alongside the results of the active-source processing in Figs. 9a–d (top). As shown, the dispersion curves estimated from the different sets of data overlap in a common frequency range of 6.8–11 Hz for Landeyjar Harbor (Fig. 9a), 7.3–10.4 Hz for Markarfljót Bridge (Fig. 9b), 12.7–25 Hz for Stóra-Laxá Bridge (Fig. 9c) and 9.1–13.9 Hz for Óseyri Bridge (Fig. 9d). Hence, the results show good agreement between the different data acquisition techniques and indicate that the active- and passive-source branches can in all cases be reasonably combined into a single broadband dispersion curve.

The variability among the extracted phase velocity values is evaluated in terms of the coefficient of variation (COV) and shown in Figs. 9a–d (bottom). Consistent with previously reported findings (Lai et al. 2005; Roy and Jakka 2018; Olafsdottir et al. 2018b; Passeri et al. 2021), the lower frequency components tend to display more variation than components in the higher frequency range. This is particularly evident for the Landeyjar Harbor, Markarfljót Bridge and Óseyri Bridge sites (Figs. 9abd). The experimental dispersion curves retrieved for these three sites all display very low COV values (COV < 0.025) at frequencies above approximately 20 Hz, which increase to 0.05–0.085 below 10 Hz. The variation within the set of dispersion curves retrieved by the Stóra-Laxá Bridge is slightly higher, however, a COV of approximately 0.05–0.10 (Fig. 9c) within the analyzed frequency range is consistent with values obtained at other sites and those reported in the literature (e.g., Passeri et al. 2021).

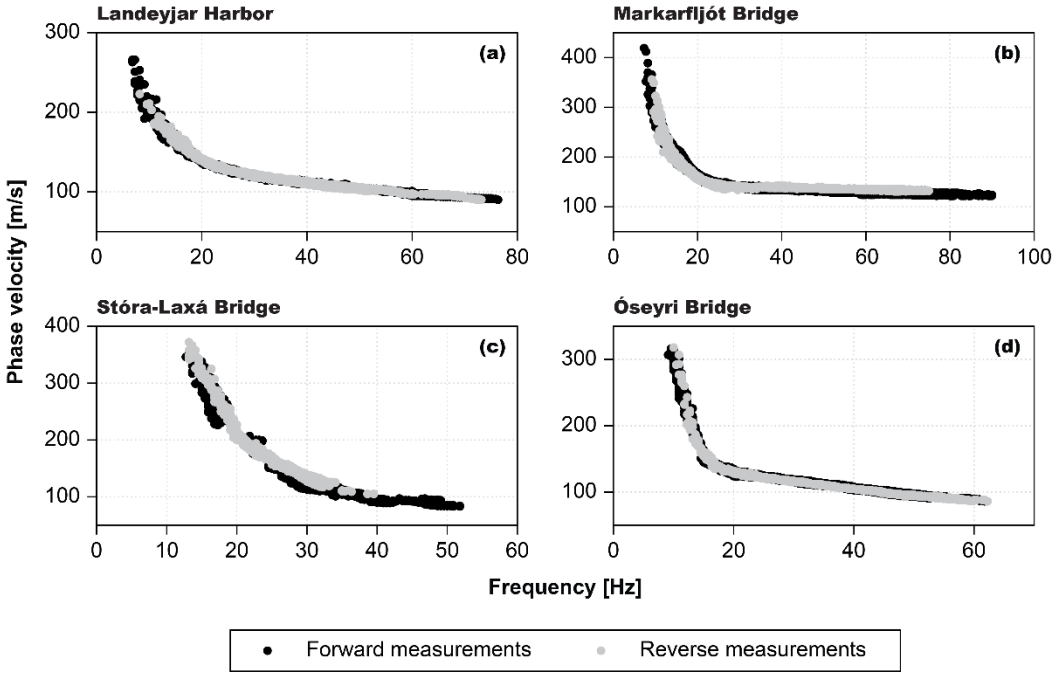


***Fig. 8*** *Experimental dispersion curves retrieved from repeated forward and reverse shot gathers (active-source measurements, MASW) acquired at the* ***a*** *Landeyjar Harbor,* ***b*** *Markarfljót Bridge,* ***c*** *Stóra-Laxá Bridge and* ***d*** *Óseyri Bridge sites*

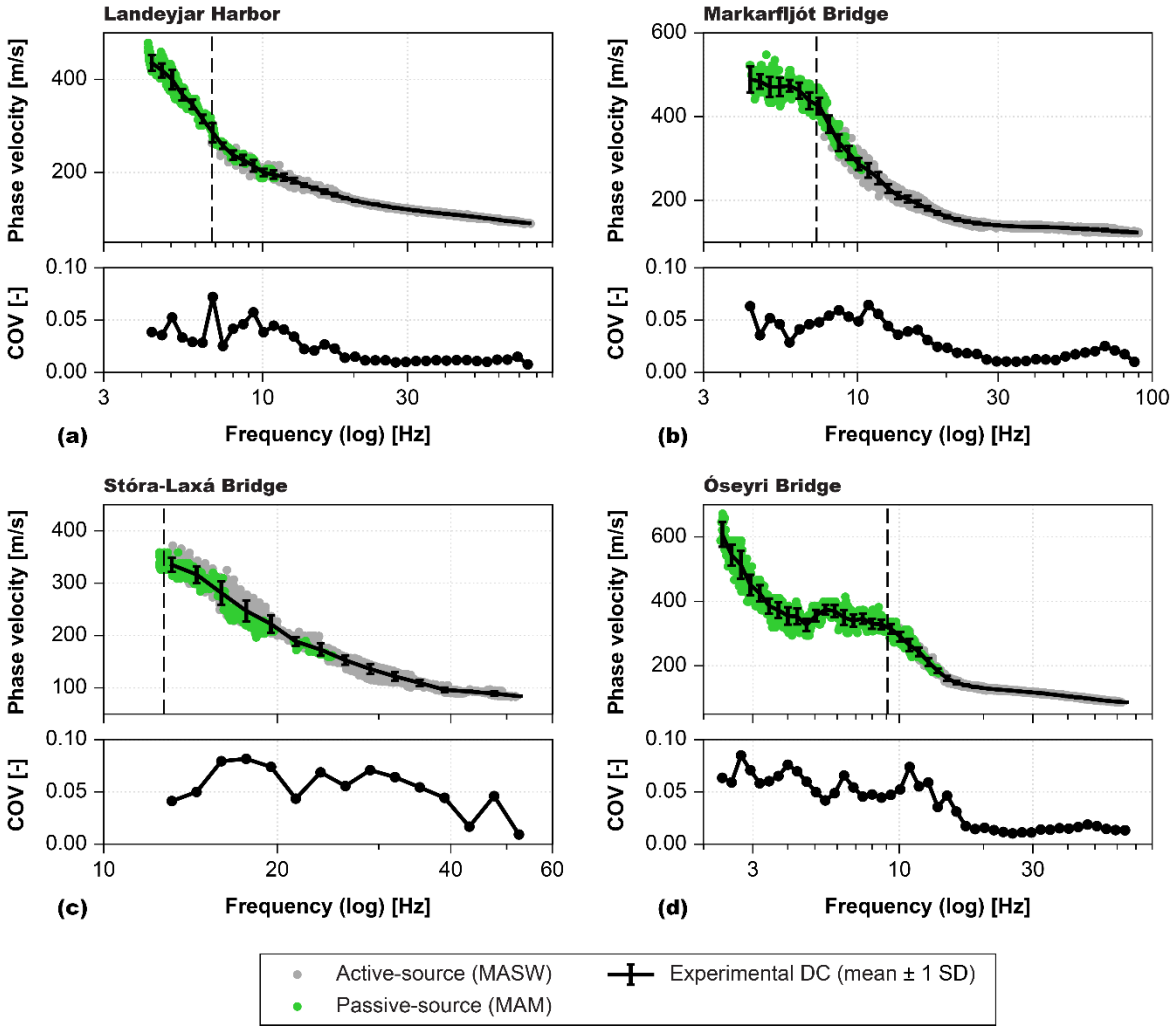


***Fig. 9*** *Experimental dispersion curves identified from active-source (MASW) and passive-source (MAM) measurements and variation (COV) of the extracted phase velocity values with frequency for the* ***a*** *Landeyjar Harbor,* ***b*** *Markarfljót Bridge,* ***c*** *Stóra-Laxá Bridge and* ***d*** *Óseyri Bridge sites. The composite dispersion curve (DC) for each site is shown with the black line and standard deviations (SD) with vertical error bars. The dashed vertical line segment shows the lower bound frequency of the contribution of the active-source data*

## 5. Evaluation of $V_S$ profiles and comparison with existing data

The hybrid inversion of the experimental dispersion and ellipticity curves was conducted by using the conditional neighborhood algorithm (NA) (Sambridge 1999; Wathelet 2008) as implemented in the Dinver module in Geopsy (Wathelet 2008; Wathelet et al. 2004, 2020). Forward computations (Wathelet 2005) are based on the transfer matrix approach of Thomson (1950) and Haskell (1953) with later modifications by Knopoff (1964), Dunkin (1965) and Herrmann (1994).

The stratigraphic structure at each site was modelled as a stack of isotropic linear-elastic layers over a half-space. The 1D model assumption is supported by the limited variability in the retrieved HVSR and ellipticity curves (Figs. 5, 6) and the consistency between the forward and reverse active-source dispersion curves at the respective sites (Fig. 8). Each layer is defined by its shear wave velocity, compressional wave velocity ($V_P$), material density ($\rho$) and thickness ($h$). As the theoretical dispersion and ellipticity curves are not strongly affected by $\rho$, the material density was fixed at 2,000 kg/m$^3$, based on typical values for sandy and gravelly soils in South Iceland. The shear and compressional wave

velocities of each layer were linked by the Poisson's ratio (confined to the range of 0.2–0.5) to prevent models with physically impossible combinations of $V_S$ and $V_P$. For layers modeled as saturated, the sampled $V_P$ values were further constrained to a minimum of 1,440 m/s. The misfit ($m$) between a theoretically computed curve and the corresponding experimental data is defined as (Wathelet et al. 2004; Hobiger et al. 2013)

$$m = \sqrt{\frac{1}{N}\sum_{i=1}^{N}\left(\frac{D_i - T_i}{E_i}\right)^2} \quad (2)$$

where $N$ is the number of frequency samples, $T_i$ and $D_i$ are the theoretical and experimental values for the $i$-th data point, respectively, and $E_i$ is the associated measurement error. Separate dispersion and ellipticity misfits were computed using Eq. (2). The sampled models were subsequently ranked by the weighted average of the two ($\overline{m}$) by imposing equal weights on the dispersion and ellipticity misfits. For each model parameterization, the NA optimization was initiated five times with 50,000–100,000 trial models sampled in each initiation. The lowest value of the dispersion-ellipticity misfit function for a given initiation is denoted as $\overline{m}_{min}$.

The lognormal median ellipticity curves obtained with the RayDec method (Fig. 7) were specified as ellipticity inversion targets. For ellipticity curves exhibiting singularities, the peak frequency and the right flank of the ellipticity peak have been shown to carry the most valuable information for development of soil $V_S$ profiles at depth (Hobiger et al. 2013). Reliable parts of the ellipticity curves for use in the inversions, primarily around the observed peaks and troughs, were identified by comparison of the RayDec and HVTFA results (Figs. 6, 7). The standard deviations of the RayDec curves primarily reflect the temporal variability of the recorded microtremors and do not account for model-based (i.e., epistemic) factors which also affect the estimated ellipticity. Therefore, to better describe the uncertainty associated with the retrieved ellipticity values, its upper and lower boundaries were specified as two standard deviations of the lognormal median curve. The boundary values of the composite dispersion curves were specified in the same way, i.e., as $E = 2 \cdot SD$ in Eq. (2). Hence, a misfit value of $\overline{m} = 1.0$ indicates that, on average, the theoretically computed dispersion and ellipticity curves fall within two standard deviations of the corresponding experimental data.

### *5.1 Sedimentary sites: Landeyjar Harbor and Markarfljót Bridge*

To first assess the performance of the hybrid analysis at locations in South Iceland with a relatively simple structure, the experimental data acquired at Landeyjar Harbor and Markarfljót Bridge, respectively, were inverted as outlined above. Limited data exists on soil layering or the presence of distinct stratigraphic units. Several different parameterizations were therefore considered for the respective sites (Table 2). The top-most layer was modelled as unsaturated and its characteristic values of $V_S$ and $V_P$ set to increase linearly in three steps. Preliminary evaluations, using Eq. (1), the estimated range for $f_{0,HV}$ and typical values of $V_S$ for basaltic sand and gravel (Erlingsson et al. 2022; Olafsdottir et al. 2022), were conducted for each site to estimate the upper boundary value of the depth to bedrock. The depth to the top of the half-space was subsequently restricted to a maximum of 300 m as the results of the preliminary evaluations indicated bedrock to be much shallower than that. No velocity reversals were considered.

***Table 2*** *Inversion targets and parameter ranges, shear wave velocity ($V_S$) and depth of layer interfaces ($z$), used for the hybrid dispersion-ellipticity inversions at the Landeyjar Harbor and Markarfljót Bridge sites*

| | **Inversion targets** | | | | | |
|---|---|---|---|---|---|---|
| | **Landeyjar Harbor (LH)** | | | **Markarfljót Bridge (MB)** | | |
| | $f$ [Hz] | Notes | | $f$ [Hz] | Notes | |
| Ellipticity curve | 0.39–0.53 | Left flank of peak | | 0.50–0.74 | Left flank of first peak | |
| | 0.72–1.21 | Right flank of peak | | 1.01–1.60 | Right flank of first peak | |
| | | | | 3.2–5.9 | Broad (non-singular) peak | |
| Dispersion curve | 4.3–74.7 | | | 4.3–87.0 | | |
| | **Four-layered system** | | **Five-layered system** | | **Six-layered system** | |
| | $V_S$ [m/s] | $z$ [m] | $V_S$ [m/s] | $z$ [m] | $V_S$ [m/s] | $z$ [m] |
| Layer 1 | 50–500(*) | 3–5 (LH)<br>2–4 (MB) | 50–500(*) | 3–5 (LH)<br>2–4 (MB) | 50–500(*) | 3–5 (LH)<br>2–4 (MB) |
| Layer 2 | 50–1500 | 2–50 | 50–1500 | 2–50 | 50–1500 | 2–50 |
| Layer 3 | 50–1500 | 2–100 | 50–1500 | 2–50 | 50–1500 | 2–50 |
| Layer 4 | 50–1500 | 2–300 | 50–1500 | 2–100 | 50–1500 | 2–100 |
| Layer 5 | | | 50–1500 | 2–300 | 50–1500 | 2–100 |
| Layer 6 | | | | | 50–1500 | 2–300 |
| Half-space | 50–3500 | - | 50–3500 | - | 50–3500 | - |

(*) Linear increase in three steps within the layer.

The ellipticity curves retrieved at the Landeyjar Harbor site (Figs. 6a, 7a) exhibit a clear peak around 0.62 Hz. The trough is identified at 1.3 Hz. Here, the right flank of the ellipticity peak is inverted, omitting ellipticity values higher than 3.2. To constrain the peak frequency, the left flank is also included in the inversion. The resulting frequency gap in the experimental data is relatively large, i.e., a factor of 3.6 (Table 2). It is, nevertheless, considered adequate because of the simple stratigraphic structure expected in the Landeyjar Harbor area. The part of the ellipticity curve beyond the trough is considered less reliable as an inversion target, both due to the more pronounced differences between the RayDec and HVTFA results (Fig. 6a), and as higher frequency ellipticity values are, in general, more prone to be affected by higher modes than those at lower frequencies.

Figure 10 summarizes the inversion results for Landeyjar Harbor. For each inversion initiation, 1,000 models were randomly selected from the subset of sampled models whose misfit values fulfil $\bar{m} \leq 1.25\bar{m}_{min}$. The resulting collection of $V_S$ profiles is shown in Fig. 10c and Fig. 10d (top 30 m) where the profiles are color-coded by their dispersion-ellipticity misfit values. Figures 10ab compare the associated set of theoretically computed ellipticity and dispersion curves, respectively, to the experimental data points specified as inversion targets. Figures 10ef further depict the lowest misfit ($\bar{m}_{min}$) $V_S$ profiles resulting from each inversion initiation. The results presented in Fig. 10 reveal a strong impedance contrast at a depth between 165 m and 190 m, which is interpreted as depth to competent bedrock. The bedrock velocity is not well constrained. Nevertheless, the inverted values are in line with typical $V_S$ for basaltic rock of 2000–2800 m/s (Sigbjörnsson and Ólafsson 2004). For the sand/gravel sediments, the developed velocity profiles indicate values of $V_S$ increasing from around 90 m/s close to surface level up to 550–600 m/s for the deep sediments, which is consistent with previous measurements at comparable sites in the area (Bessason and Erlingsson 2011; Erlingsson et al. 2022). However, for the South Iceland region as a whole, very limited comparison data exists for depths exceeding 25 m. The different layering parameterizations (Table 2) provide a similar fit between the experimental data and the theoretical curves. In particular, the ellipticity peak and trough, and the dispersion curve at frequencies above 5 Hz are consistently well matched. Although not included in the

inversion, the theoretically computed ellipticity curves also fit the experimental data well in the frequency range of 1.5–2.5 Hz (gray error bars in Fig. 10a). Extending the ellipticity inversion target to include a part of the experimental curve beyond the trough, thus reducing the frequency gap below a factor of 2 as recommended by Hobiger et al. (2013), did therefore not significantly affect the retrieved $V_S$ structure.

The inversion results for the Markarfljót Bridge site are summarized in Fig. 11. The experimental ellipticity curves retrieved at the site (Figs. 6b, 7b) show a peak at approximately 0.9 Hz, which is considered singular in the inversion. The trough frequency around 2 Hz is less apparent. The ellipticity curves further exhibit a second broad (non-singular) peak at around 4.5 Hz. The right and left flanks of the primary ellipticity peak are specified as inversion targets, omitting ellipticity values above 3.6, where the RayDec and HVTFA curves differ substantially, and values close to the implied trough. To further constrain the $V_S$ profile at shallow depths, the second peak is also included in the inversion (Table 2). The different layering parameterizations yield, overall, similar interval velocity profiles and result in comparable misfit values. The theoretically computed dispersion and ellipticity curves (Figs. 11ab) match the experimental data well over the entire frequency range and the observed ellipticity peaks and the estimated trough are consistently well retrieved. The predicted velocity profiles indicate $V_S$ in the range of 130–160 m/s for the surficial soil layers and up to around 600 m/s for the deep sediments (Figs. 11cd). Hence, compared to the Landeyjar Harbor site (Fig. 10), a slightly stiffer soil profile is retrieved, which is consistent with prior investigations and observations at the site. The velocity increase shown by the inverted $V_S$ profiles at a depth of around 17–22 m (Figs. 11df) corresponds well with the depth of the stiffer layer identified by a borehole at the site. Omitting the second (non-singular) ellipticity peak from the inversion leads to a similar velocity profile, however, the stiffness increase is less clearly constrained. Hence, the inversion results support previous conclusions relating the origin of the second ellipticity peak to the increase in stiffness detected between 15 m and 20 m depth. The depth to the top of the half-space is reasonably well constrained, therefore, based on the $V_S$ profiles showing the lowest values of the dispersion-ellipticity misfit function, the depth to bedrock is estimated to be in the range of 140–155 m.

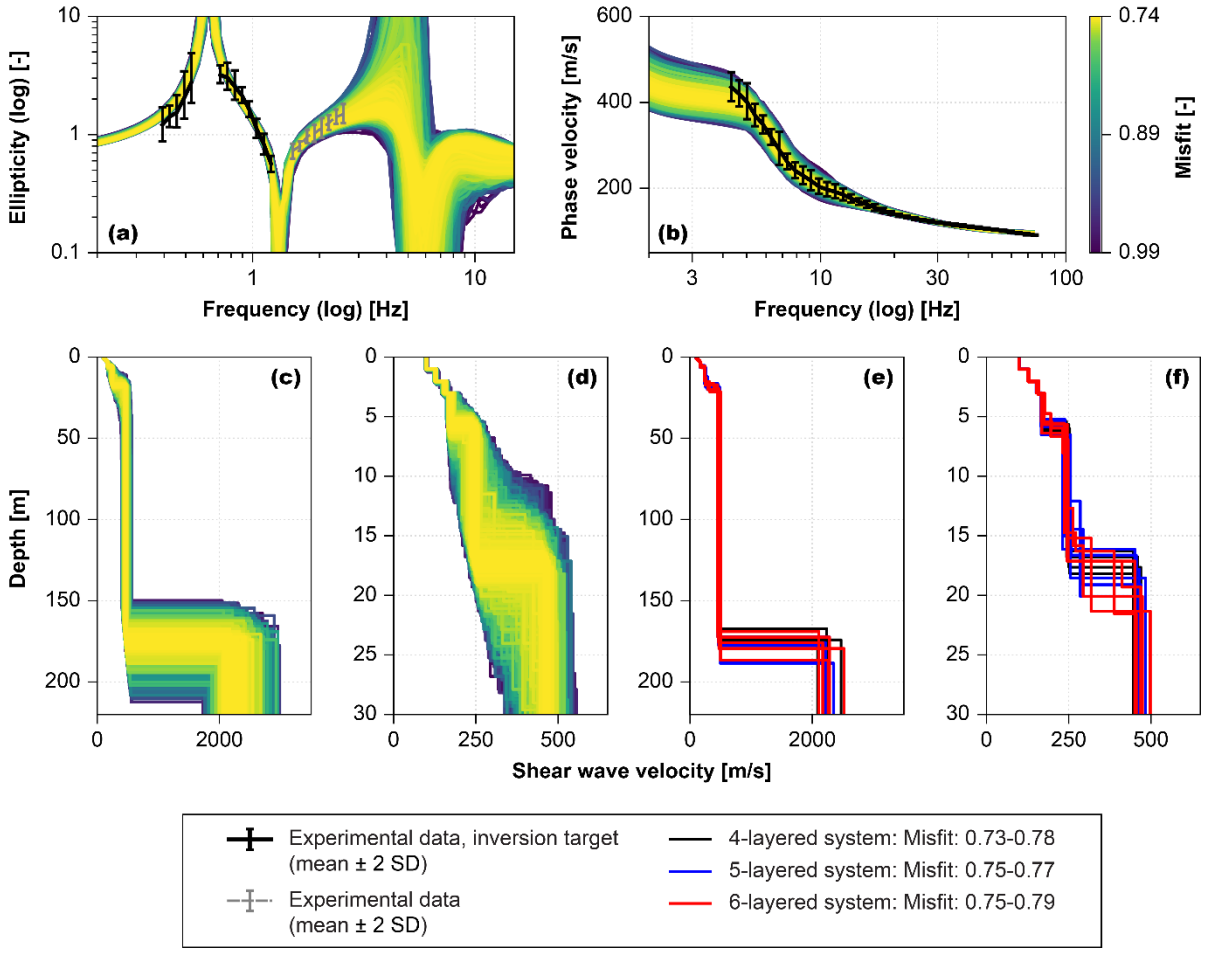


***Fig. 10*** *Results of the hybrid dispersion-ellipticity curve inversion for the Landeyjar Harbor site. For each inversion initiation (4-, 5-, or 6-layered system), 1,000 models were randomly selected from the subset of sampled models whose dispersion-ellipticity misfit values fulfil* $\overline{m} \leq 1.25\overline{m}_{min}$ *(*$\overline{m}_{min}$ *is the lowest misfit value obtained in each initiation). The resulting collection of* $V_S$ *profiles (total of 15,000 profiles) is shown in* ***c*** *(top 220 m) and* ***d*** *(top 30 m) where they are color-coded by* $\overline{m}$*. The associated set of theoretically computed ellipticity and dispersion curves is compared to the experimental data points specified as inversion targets in* ***a*** *and* ***b****. The lowest misfit (*$\overline{m}_{min}$*)* $V_S$ *profiles resulting from each inversion initiation are shown in* ***e*** *(top 220 m) and* ***f*** *(top 30 m)*

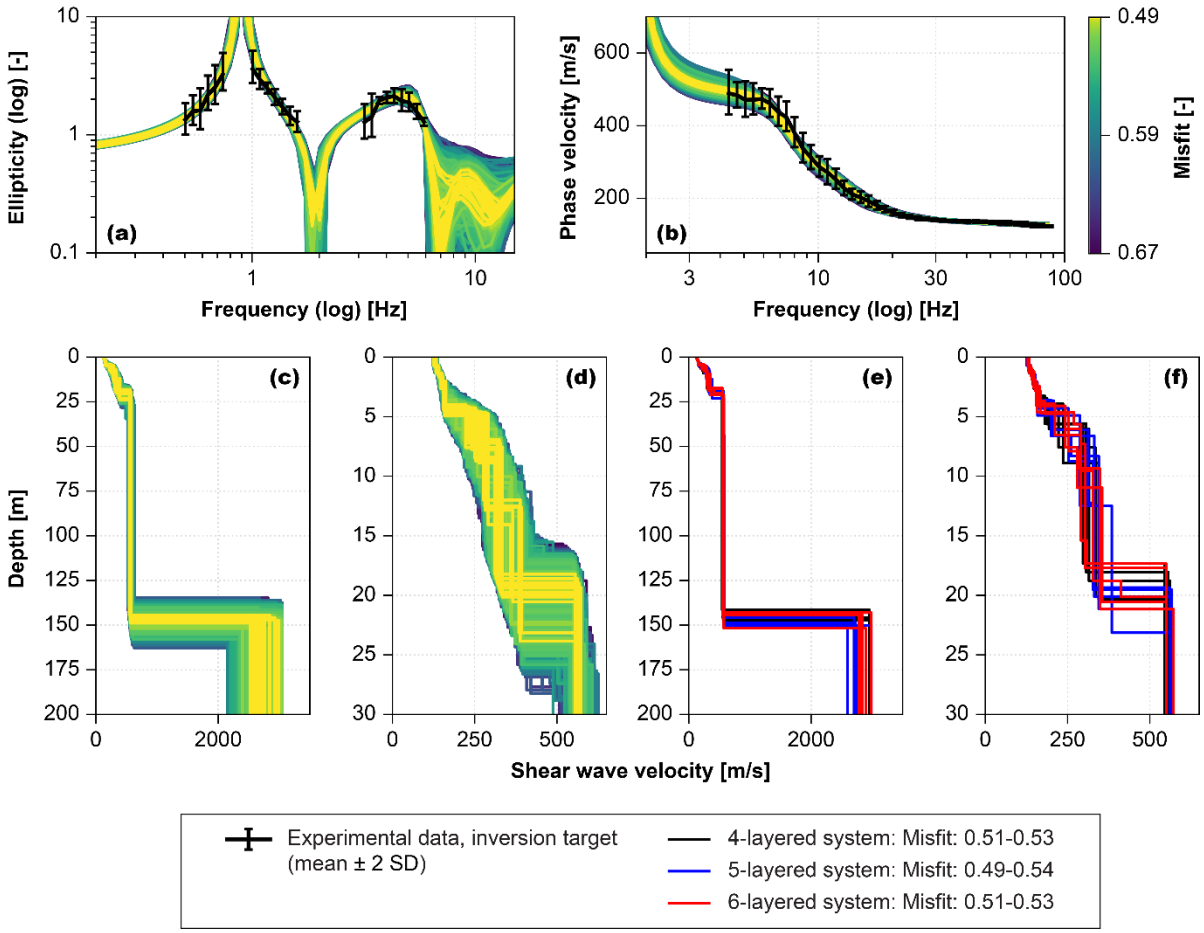


***Fig. 11*** *Results of the hybrid dispersion-ellipticity curve inversion for the Markarfljót Bridge site. The results are presented in the same manner as described for Fig. 10*

*5.2 Sedimentary/lave-rock sites: Stóra-Laxá Bridge and Óseyri Bridge*

To initially test the applicability of the hybrid inversion routine for sedimentary/lava-rock sites, the experimental dispersion and ellipticity data retrieved by the Stóra-Laxá Bridge was inverted. Based on the available data and initial sensitivity analysis, the site was modelled as a four-layered system over a half-space representing bedrock (Table 3), with a velocity reversal permitted between layers 3 and 4. Preliminary estimations, using the estimated range for $f_{1,HV}$ and maximum $V_S$ values for the expected surficial soils (Erlingsson et al. 2022), were used to specify the maximum depth of the interface between layers 2 and 3. Hence, during the inversion process, the depth and thickness of the intermittent scoria layer were allowed to vary substantially beyond the known geology at the site. Little information exists on typical $V_S$ values for scoria or other types of lava-rock found in the South Iceland Lowland. However, as the lava is typically highly fractured, its $V_S$ is expected to be somewhat lower than values reported for basaltic rock. Existing studies have used values of 1000 m/s (Bessason and Kaynia 2002) and 1800 m/s (Rahpeyma et al. 2016). An average $V_S$ of tuff (i.e., lithified volcanic ash) has further been reported as 850 m/s (Sigbjörnsson and Ólafsson 2004). Here, an upper range value of 2000 m/s was specified for the scoria layer. Increasing it to 2500 m/s was not found to provide a better fit to the experimental data. The upper boundary value of the depth to underlying bedrock was estimated in the same way as described in the preceding section.

***Table 3*** *Inversion targets, parameter ranges, shear wave velocity ($V_S$) and depth of layer interfaces ($z$), used for the hybrid dispersion-ellipticity inversions at the Stóra-Laxá Bridge site*

| | **Inversion targets** | |
|---|---|---|
| | $f$ [Hz] | Description |
| Ellipticity curve | 2.2–2.9 | Left flank of first peak |
| | 4.2–5.3 | Right flank of first peak |
| | 6.4–8.2 | Left flank of second peak |
| | 9.9–11.1 | Right flank of second peak |
| Dispersion curve | 13.4–52.5 | |
| | **Four-layered system** | |
| | $V_S$ [m/s] | $z$ [m] |
| Layer 1 | 50–500 | 1–2 |
| Layer 2 | 50–500 | 1–10 |
| Layer 3 | 50–2000$^{(+)}$ | 1–25 |
| Layer 4 | 50–3500$^{(+)}$ | 1–100 |
| Half-space | 50–3500 | - |

$^{(+)}$ Velocity reversal permitted between the two layers.

The inversion results for the Stóra-Laxá Bridge site are presented in Fig. 12. The shaded area in Figs. 12df represents the depth and thickness of the scoria layer, as established by the T-13 and T-15 boreholes (Fig. 2). To constrain the frequencies of both ellipticity peaks, four segments of the retrieved ellipticity were specified as inversion targets (Table 3). This results in a frequency gap of a factor of 1.2 between the ellipticity data and the dispersion curve for the site. The ellipticity and dispersion curves resulting from the inversion (Fig. 12ab) fit the experimental data well over the entire analyzed frequency range. The observed peaks in the ellipticity curves at 3.1–3.3 Hz and around 9 Hz, and the trough between 5 Hz and 6 Hz are further consistently retrieved by the theoretical curves.

The resulting interval velocity profiles indicate a $V_S$ of approximately 85 m/s close to surface. It then increases to around 180 m/s at 5 m depth. Previous SWM at gravelly sites in South and South-West Iceland have indicated comparable values within the top 5 m (Bessason and Erlingsson 2011; Erlingsson et al. 2022). The inverted $V_S$ values are further in line with those predicted for the surficial soil sediments by the Landeyjar Harbor and Markarfljót Bridge (Figs. 10df, 11df), which also primarily consist of basaltic sand and gravel. The inversion results show a sharp velocity increase at a depth of 5–6 m, which is consistent with the top of the scoria layer. The sharp velocity decrease at around 13 m depth, interpreted as the interface between the scoria and the underlying layers of gravel, sand and silt, is further consistent with the available data. Beneath the scoria, the results presented in Fig. 12 indicate $V_S$ of 280–400 m/s. Limited information exists on typical $V_S$ values of soft sediments underlying lava-rock. At a depth of 15–20 m, previous measurements at sandy and gravelly sites in the South Iceland Lowland (Erlingsson et al. 2022) have indicated a $V_S$ typically in the range of 200–400 m/s, although examples of both higher and lower $V_S$ within this depth range exist. The overburden of the scoria is further expected to somewhat increase the stiffness of the underlying sediments, as compared to sites without this overburden. The second strong impedance contrast at around 35 m depth is interpreted as depth to underlying bedrock. As the estimated depth to bedrock is less than at the other research sites, only the top 55 m of the inverted $V_S$ profiles are shown in Fig. 12.

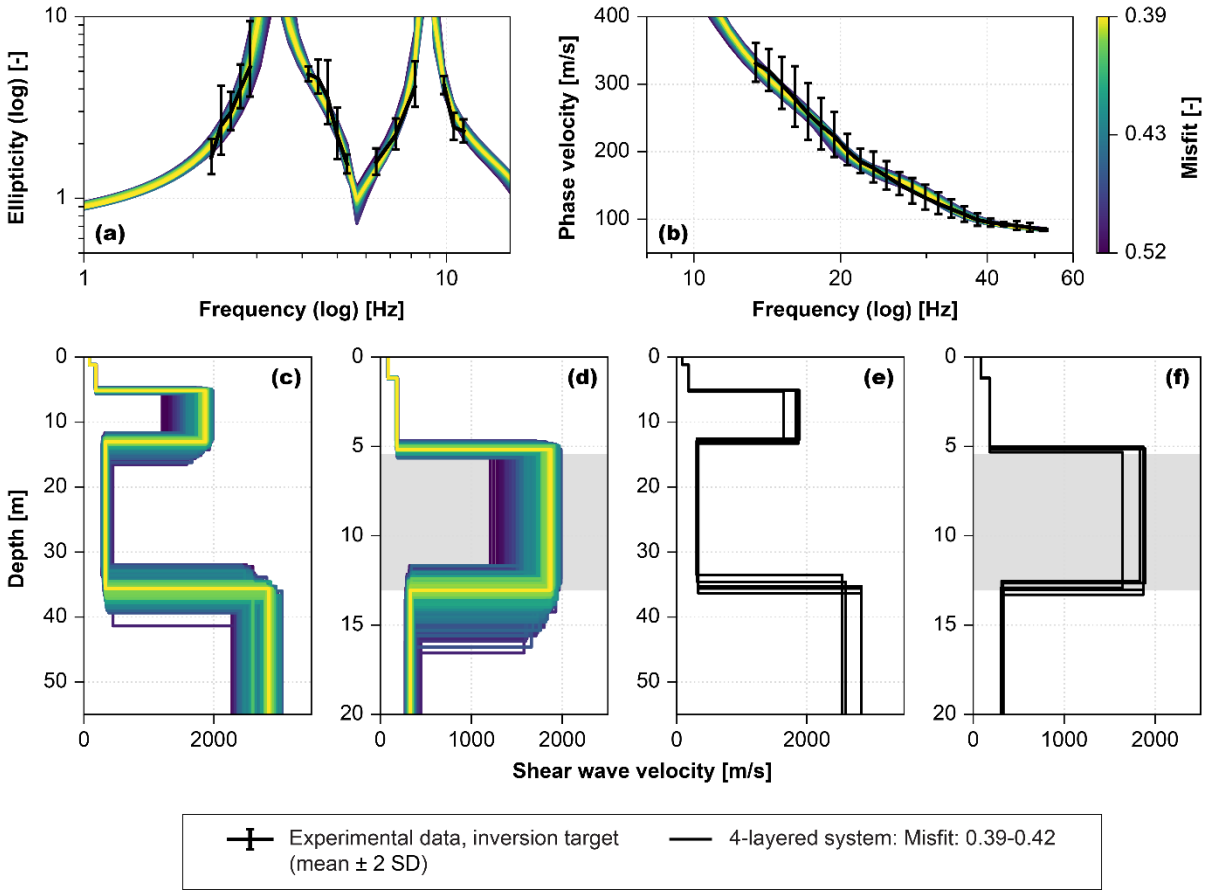


***Fig. 12*** *Results of the hybrid dispersion-ellipticity curve inversion for the Stóra-Laxá Bridge site. For each inversion initiation (4-layered system), 1,000 models were randomly selected from the subset of sampled models whose misfit values fulfil* $\overline{m} \leq 1.25\overline{m}_{min}$*. The resulting collection of* $V_S$ *profiles (total of 5,000 profiles) is shown in* ***c*** *and* ***d****. The associated set of theoretical ellipticity and dispersion curves is compared to the experimental data in* ***a*** *and* ***b****. The lowest misfit* $V_S$ *profiles resulting from each of the five initiations are shown in* ***e*** *and* ***f****. The gray shaded area in* ***d*** *and* ***f*** *represents the depth and thickness of the scoria layer, as established by the T-13 and T-15 boreholes*

Based on the similarities between the ellipticity curves retrieved at the Stóra-Laxá Bridge and Óseyri Bridge sites, the Óseyri Bridge inversion was also initiated by assuming a four-layer subsoil structure above a half-space (Table 4), with a velocity reversal permitted between layers 3 and 4. The maximum depth to the top of layer 3 and the depth to the half-space top were specified in a comparable manner as for the Stóra-Laxá Bridge inversion. To retrieve more details on the soil layer structure, and to better fit the experimental dispersion curve at higher frequencies, the seismic wave velocities within the unsaturated surficial layer were allowed to increase linearly in three steps.

***Table 4*** *Inversion targets and parameter ranges, shear wave velocity ($V_S$) and depth of layer interfaces ($z$), used for the hybrid dispersion-ellipticity inversions at the Óseyri Bridge site*

| | **Inversion targets** | | | | | |
|---|---|---|---|---|---|---|
| | $f$ [Hz] | Description | | | | |
| Ellipticity curve | 0.56–1.0 | Left flank of first peak | | | | |
| | 1.34–2.23 | Right flank of first peak | | | | |
| | 4.3–5.8 | Left flank of second peak | | | | |
| | 7.2–10.3 | Right flank of second peak | | | | |
| Dispersion curve | 2.4–64.0 | | | | | |
| | **Four-layered system** | | **Five-layered system, above** | | **Five-layered system, below** | |
| | $V_S$ [m/s] | $z$ [m] | $V_S$ [m/s] | $z$ [m] | $V_S$ [m/s] | $z$ [m] |
| Layer 1 | 50–500(*) | 2–4 | 50–500(*) | 2–4 | 50–500(*) | 2–4 |
| Layer 2 | 50–500 | 2–15 | 50–500 | 2–15 | 50–500 | 2–15 |
| Layer 3 | 50–2000(+) | 2–30 | 50–500 | 2–15 | 50–2000(+) | 2–30 |
| Layer 4 | 50–3500(+) | 2–120 | 50–2000(+) | 2–30 | 50–3500(+) | 2–120 |
| Layer 5 | | | 50–3500(+) | 2–120 | 50–3500 | 2–120 |
| Half-space | 50–3500 | - | 50–3500 | - | 50–3500 | - |

(*) Linear increase in three steps within the layer.
(+) Velocity reversal permitted between the two layers.

Figure 13 presents the joint inversion of the broadband dispersion curve (Fig. 9d) and the ellipticity data (Fig. 7d) for the Óseyri Bridge site. The experimental ellipticity curve displays two distinct peaks that are both considered singular. Hence, four segments of the observed ellipticity were specified as inversion targets (Table 4), omitting the ellipticity values around the peaks and troughs. As a result, the dispersion and ellipticity data overlap between 2.4 Hz and 10.3 Hz. The theoretically computed dispersion and ellipticity curves (Fig. 13ab) fit the experimental data well over the entire frequency range, and the two ellipticity peaks at around 1.15 Hz and 6.6 Hz, and the trough at 2.4 Hz, are consistently well reproduced. The developed velocity profiles indicate the presence of a stiff inclusion layer in the soil strata between depths of approximately 6 m and 12–13 m. No direct measurements of the thickness of the surficial sediments by the Óseyri Bridge exist. However, a sediment thickness of around 6 m is in line with data collected in conjunction with the design of the Óseyri Bridge (Icelandic Road Administration 1986). Based on the collection of profiles shown in Fig. 13, the characteristic $V_S$ value of the stiff layer is estimated to be in the range of 800–900 m/s. The resulting $V_S$ estimates for the sediment layers are, overall, in line with those retrieved for the Stóra-Laxá Bridge site. The large impedance contrast at a depth of around 80 m, related to the first peak of the ellipticity curve, is interpreted as depth to underlying bedrock. Adding a layer to the soil model, either above or below the stiff (lava-rock) layer (Table 4) yields a comparable fit to the experimental data and provides a very similar estimate of the $V_S$ profile as was obtained by assuming the simpler four-layer model (Figs. 13ef).

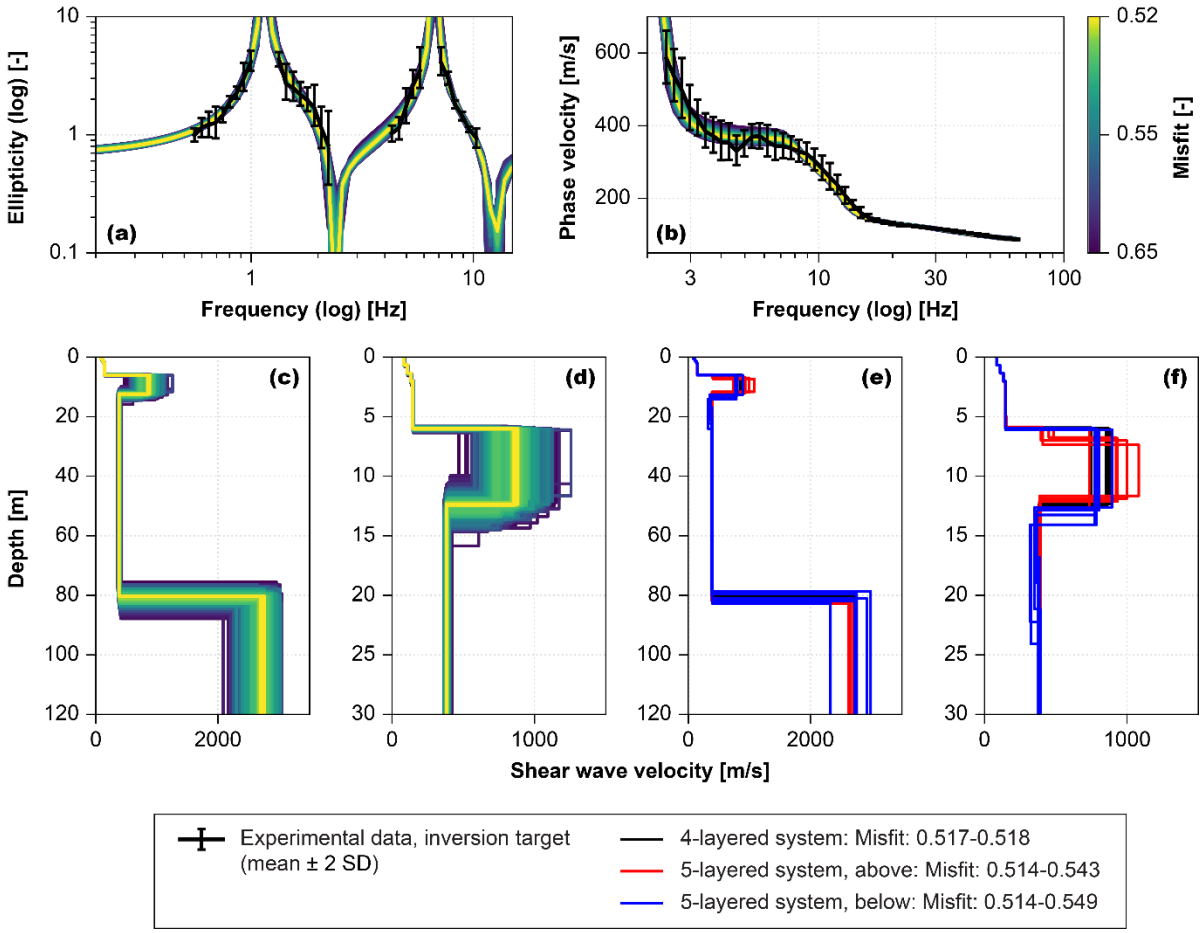


***Fig. 13*** *Results of the hybrid dispersion-ellipticity curve inversion for the Óseyri Bridge site. For each inversion initiation (4-layered system), 1,000 models were randomly selected from the subset of sampled models whose misfit values fulfil* $\bar{m} \leq 1.25\bar{m}_{min}$. *The resulting collection of* $V_S$ *profiles (total of 5,000 profiles) is shown in* ***c*** *and* ***d***. *The associated set of theoretical ellipticity and dispersion curves is compared to the experimental data in* ***a*** *and* ***b***. *The lowest misfit* $V_S$ *profiles resulting from each initiation are shown in* ***e*** *and* ***f*** *(black lines).* ***e*** *and* ***f*** *further show the lowest-misfit* $V_S$ *profiles obtained by modeling the site as a 5-layered system, with an additional layer either added above (red lines) or below (blue lines) the rock layer*

### *5.3 Summary of modelling results*

The main results of the site characterization for the four sites are summarized in Table 5. For the two sites without an embedded rock layer (i.e., the soil sites) $H_{800}$ is the depth to the seismic bedrock formation as defined in the 2021-draft of Eurocode 8 (Paolucci et al. 2021) and $H$ = 30 m if $H_{800}$ > 30 m. For the embedded lava-rock sites $H1_{rock}$ is the depth to the embedded rock layer, $h_{rock}$ is the thickness of the embedded rock and $H2_{800}$ is the depth to underlying seismic bedrock.

***Table 5*** *Summary of the site characterization for the four test sites*

| **Type** | | | **Landeyjar Harbor** | **Markarfljót Bridge** | **Stóra-Laxá Bridge** | **Óseyri Bridge** |
|---|---|---|---|---|---|---|
| Soil site | $V_{S,30}$ | [m/s] | 260 | 305 | | |
| | $H$ | [m] | 30 | 30 | | |
| | $H_{800}$ | [m] | 165–190 | 140–155 | | |
| Embedded lava-rock site | $V_{S,H1}$ | [m/s] | | | 145 | 130 |
| | $H1_{rock}$ | [m] | | | 4.5–5.5 | 6 |
| | $h_{rock}$ | [m] | | | 7–8 | 6–7 |
| | $H2_{800}$ | [m] | | | 35 | 80 |

## 6. Discussion

In previous studies, HVSR curves exhibiting two distinct peaks have been associated with the presence of two significant impedance contrasts at different depths (SESAME 2004; Hunter et al. 2020; Molnar et al. 2022). Bimodal HVSR curves, retrieved at a known lava-rock/sedimentary site in South Iceland, have been interpretated as the response of a structure consisting of two sets of lava-sedimentary layers above bedrock (Rahpeyma et al. 2016). In addition, unimodal amplification curves have been observed at a site where soft sediments are known to be sandwiched between a surficial lava-rock layer and bedrock (Bessason and Kaynia 2002). The current study adds to this by demonstrating that bimodal microtremor HVSR obtained at sedimentary sites in the South Iceland Lowland can be used to indicate the presence of a lava-rock layer embedded in the sedimentary stratum.

Moreover, the hybrid dispersion-ellipticity curve inversion has shown a potential to retrieve the depth and thickness of the embedded lava-rock layer, as well as to provide realistic estimates of $V_S$ for both the surficial and underlying sediments. The depth to the underlying bedrock is also of interest for seismic site characterization and assessment of site effects. No independent estimates of the depth to the bedrock formation exist for the two sedimentary/lava-rock sites considered in this work. Therefore, the ability of the hybrid analysis to accurately retrieve the depth to bedrock is uncertain. Very limited information exists on typical $V_S$ values for different types of Icelandic lava-rock. A large variation is further expected due to the irregularity and inhomogeneity of igneous rock structures. Hence, the estimated $V_S$ of the lava-rock layers cannot be verified by comparison with existing data. A previous numerical study on site amplifications where lava-rock overlies soft sediments (Bessason and Kaynia 2002) found that the average $V_S$ of the underlying sediments is the primary factor controlling the computed site response and that different $V_S$ gradients within the sedimentary layer provided approximately the same results. The stiffness of the lava-rock layer was not found to have a significant effect on the computed site response, given that its $V_S$ was significantly higher than that of the underlying sediments. Thus, for the purpose of seismic site response analysis, accurate evaluation of the dynamic properties of the lava-rock is not considered a priority. The findings of Bessason and Kaynia (2002) are further considered to justify the simplified four-layer model adopted for the two sedimentary/lava-rock sites (Figs. 12 and 13), particularly, the constant $V_S$ of the loose sediments beneath the lava-rock.

An important consideration when preparing in-situ SWM is determining the frequency range of the experimental data required to reliably reproduce the velocity profile down to a sufficient depth. Hobiger et al. (2013) found that for hybrid dispersion-ellipticity inversion, a frequency gap may be present between the measured dispersion and ellipticity curves. Without a-priori knowledge of the stratigraphic structure, their resulting general recommendation was to limit the maximum width of the frequency gap to a factor of 2, although a larger gap may be sufficient for simple structures. For characterization of sites that are geologically similar to the Landeyjar Harbor and Markarfljót Bridge sites, a broadband dispersion curve is therefore required to both provide a sufficient link to the ellipticity data at low frequencies and to constrain the stiffness properties of the surficial soil layers. In practice, this can, e.g.,

be achieved with a composite active- and passive-source survey with comparable array sizes and geophone natural frequencies as used here. The existing recommendations were, however, primarily made in the context of unimodal ellipticity curves. Therefore, their applicability for characterization of sites with an embedded layer of lava-rock at shallow depth is more uncertain.

To study which part of the dispersion curve is required to identify the depth and thickness of the lava-rock layer, the inversions for the Stóra-Laxá Bridge and Óseyri Bridge sites were repeated by gradually increasing the dispersion curve lower bound frequency and, thus, the frequency gap between the dispersion and ellipticity data. The results are shown in Figs. 14 and 15, respectively. The dashed horizontal lines show the identified upper and lower boundaries of the lava-rock layer, as given in Table 5 and shown in Figs. 12ef and 13ef. For the Stóra-Laxá Bridge site, the gray shaded area in Fig. 14 indicates the depth and thickness of the scoria layer, as established by the T-13 and T-15 boreholes. For reference, the broadband dispersion curve used in the initial inversions for each site is shown as a dashed line.

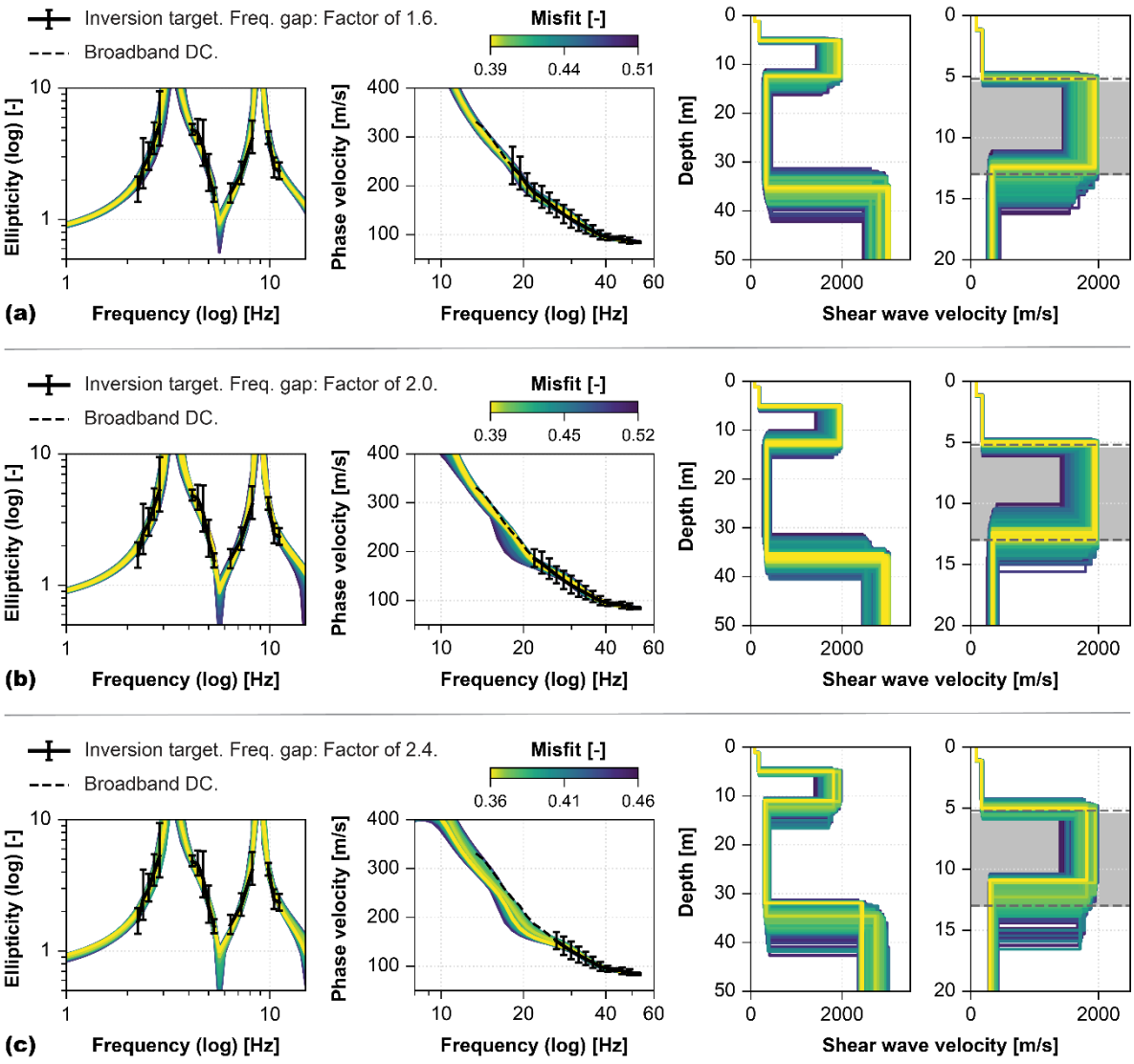


***Fig. 14*** *Inversion for the Stóra-Laxá Bridge site. Effects of increasing the frequency gap between the ellipticity and dispersion data to* ***a*** *a factor of 1.6,* ***b*** *a factor of 2.0, and* ***c*** *a factor of 2.4. The gray shaded area shown in the figures furthest to the right represents the depth and thickness of the scoria layer, as established by the T-13 and T-15 boreholes. The dashed horizontal lines also shown at depths*

*of 5.2 m and 13 m indicate the boundaries of the lava-rock layer as established by the inversion results in Fig. 12*

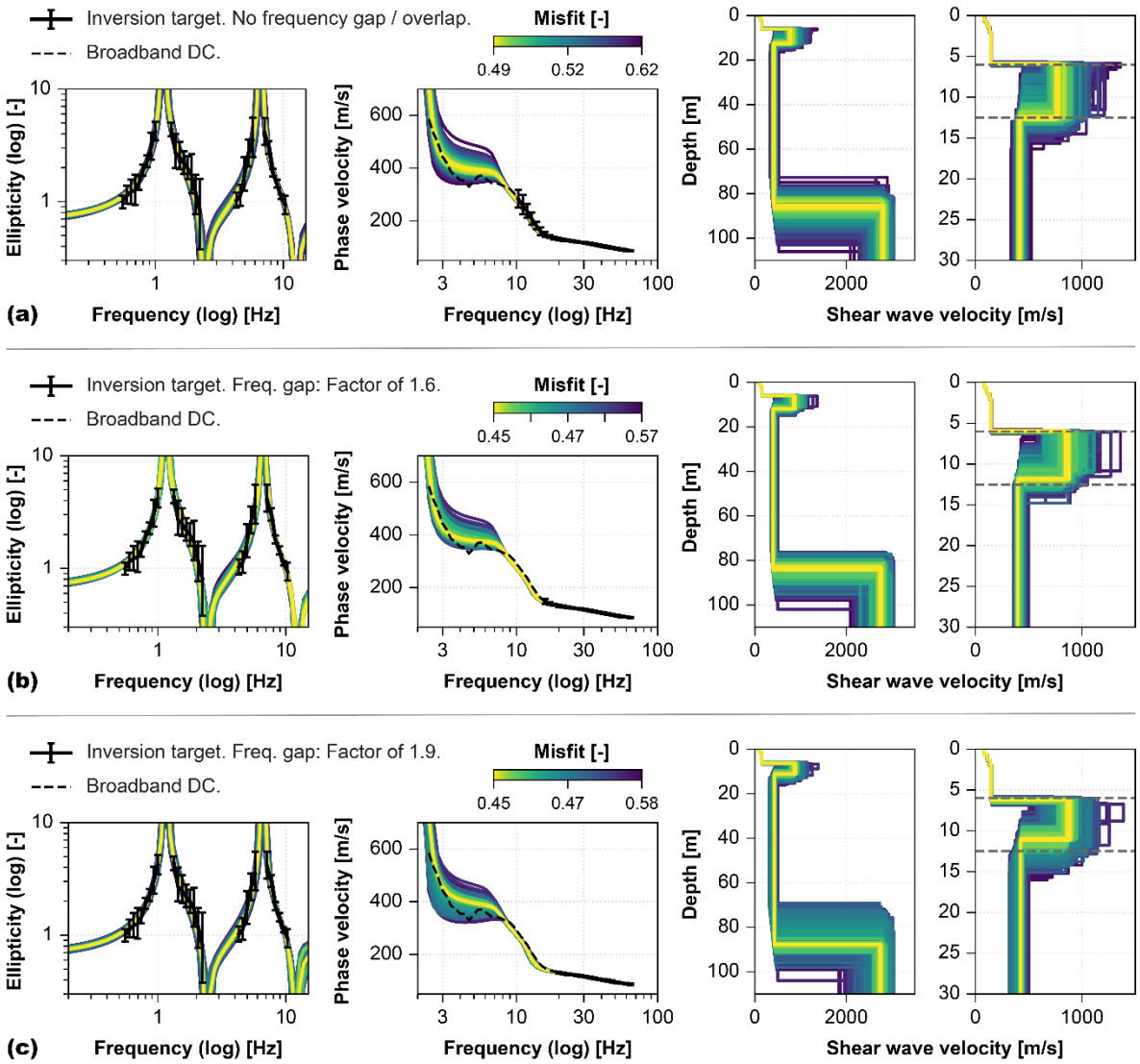


***Fig. 15*** *Inversion for the Óseyri Bridge site. Effects of* ***a*** *removing the frequency overlap in the experimental data and subsequently increasing the frequency gap between the different types of data to* ***b*** *a factor of 1.6, and* ***c*** *a factor of 1.9. The dashed horizontal lines shown in the figures furthest to the right at depths of 6 m and 12.5 m indicate the boundaries of the lava-rock layer as established by the inversion results in Fig. 13*

The results presented in Figs. 14 and 15 indicate that a frequency gap between the dispersion and ellipticity data of up to a factor of 1.5–2 does not significantly affect the ability of the hybrid inversion to correctly identify the depth and thickness of the lava-rock layer in these two cases. Widening the frequency gap beyond a factor of 1.5–2 still adequately predicts the presence of the lava-rock for both sites. However, a wider gap tends to suggest a slightly thinner lava-rock layer than is indicated by the base-line cases and available borehole data. Further increasing the frequency gap to a factor of 3 does not significantly alter the inversion results, as compared to the results shown in Figs. 14c and 15c. For the Óseyri Bridge site, removing the frequency overlap in the experimental data, also leads to a less

constrained and slightly increased estimate of the depth to underlying bedrock, i.e., a value of $H2_{800}$ in the range of 85–90 m, as compared to 80 m (Table 5). However, as no independent estimates of $H2_{800}$ exist for the site, it is impossible to evaluate whether a value of 80 m or 90 m is more accurate.

The results presented here support the conclusion of Hobiger et al. (2013) that a small frequency gap may be present in the experimental data. Nevertheless, for the purpose of constraining a layer of lava-rock that is sandwiched between soft sediments at shallow depth, the frequency gap should ideally be somewhat smaller than for sites showing a primarily unimodal ellipticity curve. Being able to omit the lowest frequency segment of the dispersion curve, without compromising on the accuracy of $H1_{rock}$ and $h_{rock}$, is considered highly beneficial from a practical perspective. It means that an active-source and/or a passive-source survey with a small-aperture array is sufficient to retrieve the dispersion curve for hybrid analysis of such sites. This makes the data acquisition more efficient and less prone to be affected by local irregularities, e.g., varying thickness of the lava-rock layer, as compared to surveys using large-aperture arrays. Furthermore, at sites with a complex geological structure, it can be difficult to confidently pick modal dispersion curves at low frequencies which, if incorrectly identified, can bias the resulting velocity profiles.

## 7. Conclusions

This study demonstrates the feasibility of a composite dispersion and ellipticity curve analysis, accompanied by microtremor HVSR, for characterization of two of the most common soil site structures in the South Iceland Seismic Zone; thick alluvial sediments overlying bedrock and sites where a layer of lava-rock is sandwiched between sedimentary layers at shallow depth.

Microtremor HVSR is found to be a highly valuable tool to distinguish between sedimentary sites with and without an embedded lava-rock layer in a fast and cost-efficient manner. At the two sites where a layer of fractured lava-rock is present in the sedimentary soil strata, the two abrupt velocity contrasts result in a clearly bimodal amplification curve. Therefore, the results suggest that microtremor HVSR should be adopted as an initial geological survey tool in the SISZ to identify sites where a layer of lava-rock may be embedded in the soil strata and more detailed surveying is therefore required.

The potential for single-station ellipticity measurements, accompanied by MASW and/or MAM testing, to characterize soil sites with embedded layers of fractured lava-rock at shallow depth is essential for subsequent studies on seismic site response in the area. The hybrid dispersion-ellipticity inversion was also found to be efficient for deep soil site characterization at sedimentary sites with a simpler structure, which is consistent with previous findings in the literature. Furthermore, at one of the tested sites, including a higher-frequency non-singular ellipticity peak in the inversion was found beneficial to help constrain a sharp velocity increase within the sedimentary strata. For the two sedimentary/lava-rock sites considered in this work, the hybrid analysis successfully retrieved the presence of the stiff lava-rock layer embedded in the softer sedimentary stratum. The predicted depth and thickness of the lava-rock at each site agrees with available geological information and existing borehole data. The estimated range in $V_S$ for the alluvial sediments is further consistent with measured values for comparable soil types found in other locations in the South Iceland Lowland.

The results presented in this work indicate that for the two sedimentary/lava-rock sites, a frequency gap between the dispersion and ellipticity data up to a factor of 1.5–2 does not have a significant effect on the ability of the hybrid inversion to identify the depth and thickness of the lava-rock layer. For sandwiched sites where the surficial sediments are relatively thin and the second ellipticity peak occurs at a comparable frequency as seen here, this means that it may be sufficient to only retrieve the mid-to-high frequency segment of the dispersion curve to successfully conduct hybrid dispersion-ellipticity analysis as described here. In practice, this is a highly useful conclusion for selection of a suitable surface wave analysis approach and array layouts.

**References**


Aki K (1957) Space and time spectra of stationary stochastic waves, with special reference to microtremors. B Earthq Res Inst 35:415–456

Akın Ö, Sayıl N (2016) Site characterization using surface wave methods in the Arsin-Trabzon province, NE Turkey. Environ Earth Sci 75:72. https://doi.org/10.1007/s12665-015-4840-6

Arai H, Tokimatsu K (2005) S-wave velocity profiling by joint inversion of microtremor dispersion curve and horizontal-to-vertical (H/V) spectrum. B Seismol Soc Am 95(5):1766–1778. https://doi.org/10.1785/0120040243

Asmussen JC (1997) Modal Analysis Based on the Random Decrement Technique: Application to Civil Engineering Structures. Dissertation, Aalborg University

Assaf J, Molnar S, El Naggar MH, Sirohey A (2022) Seismic site characterization in Fraser River Delta in Metropolitan Vancouver. Soil Dyn Earthq Eng 161:107384. https://doi.org/10.1016/j.soildyn.2022.107384

Atakan K, Brandsdóttir B, Halldórsson P, Friðleifsson GO (1997) Site response as a function of near-surface geology in the South Iceland Seismic Zone. Nat Hazards 15(2–3):139–164. https://doi.org/10.1023/A:1007902419241

Bessason B, Bjarnason JÖ (2016) Seismic vulnerability of low-rise residential buildings based on damage data from three earthquakes ($M_w$6.5, 6.5 and 6.3). Eng Struct 111:64–79. https://doi.org/10.1016/j.engstruct.2015.12.008

Bessason B, Erlingsson S (2011) Shear wave velocity in surface sediments. Jökull 61:51–64.

Bessason B, Kaynia AM (2002) Site amplification in lava rock on soft sediments. Soil Dyn Earthq Eng 22(7):525–540. https://doi.org/10.1016/S0267-7261(02)00035-0

Bessason B, Baldvinsson GI, Thórarinsson Ó (1998) SASW for evaluation of site-specific earthquake excitation. Proceedings of the 11th European Conference on Earthquake Engineering, Paris, France

Bessason B, Hafliðason E, Guðmundsson GV (2019) Performance of Base Isolated Bridges in Recent South Iceland Earthquakes. In: Rupakhey R, Olafsson S, Bessason B (eds) Proceedings of the International Conference on Earthquake Engineering and Structural Dynamics. Springer, Cham, pp 123–135. https://doi.org/10.1007/978-3-319-78187-7_10

Bessason B, Rupakhety R, Bjarnason JÖ (2022) Comparison and modelling of building losses in South Iceland caused by different size earthquakes. J Build Eng 46:103806. https://doi.org/10.1016/j.jobe.2021.103806

Bettig B, Bard PY, Scherbaum F, Riepl J, Cotton F, Cornou C, Hatzfeld D (2001) Analysis of dense array noise measurements using the modified spatial auto-correlation method (SPAC). Application to the Grenoble area. Bolletino di Geofisica Teorica ed Applicata 42(3–4):281–304

Boaga J, Cassiani G, Strobbia CL, Vignoli, G (2013) Mode misidentification in Rayleigh waves: Ellipticity as a cause and a cure. Geophysics 78(4):EN17-EN28. https://doi.org/10.1190/geo2012-0194.1

BSSC (2020) NEHRP Recommended Seismic Provisions for New Buildings and Other Structures, 2020 edition, vol. 1. Washington, DC, Building Seismic Safety Council

Castellaro S, Mulargia F (2009) VS30 estimates using constrained H/V measurements. B Seismol Soc Am 99(2A):761–773. https://doi.org/10.1785/0120080179

CEN (2004) Eurocode 8: Design of structures for earthquake resistance. Part 1: General rules, seismic actions and rules for buildings. Brussels, Belgium, European Committee for Standardization

Clifton A, Einarsson P (2005) Styles of surface rupture accompanying the June 17 and 21, 2000 earthquakes in the South Iceland Seismic Zone. Tectonophysics 396(3–4):141–159. https://doi.org/10.1016/j.tecto.2004.11.007

Dunkin JW (1965) Computation of modal solutions in layered, elastic media at high frequencies. B Seismol Soc Am 55(2):335–358. https://doi.org/10.1785/BSSA0550020335

Einarsson P (1991) Earthquakes and present-day tectonism in Iceland. Tectonophysics 189(1–4):261–279. https://doi.org/10.1016/0040-1951(91)90501-I

Einarsson P (2008) Plate boundaries, rifts and transforms in Iceland. Jökull 58:35–58

Einarsson P (2010) Mapping of Holocene surface ruptures in the South Iceland Seismic Zone. Jökull 60:117–134

Einarsson Th (1994) Geology of Iceland: rocks and landscape. Reykjavik, Mál og menning

Endrun B (2011) Love wave contribution to the ambient vibration H/V amplitude peak observed with array measurements. J Seismol 15:443–472. https://doi.org/10.1007/s10950-010-9191-x

Erlingsson S (2019) Geotechnical Challenges in Iceland. Proceedings of the XVII European Conference on Soil Mechanics and Geotechnical Engineering, Reykjavik, Iceland, pp 27–51. https://doi.org/10.32075/17ECSMGE-2019-1109

Erlingsson S, Olafsdottir EA, Bessason B (2022) Soil site stiffness categorization based on MASW field testing. Proceedings of the 20th International Conference on Soil Mechanics and Geotechnical Engineering, Sidney, Australia, pp 371–376

Fäh D, Wathelet M, Kristekova M, Havenith H, Endrun B, Stamm G, Poggi V, Burjanek J, Cornou C (2009) Using Ellipticity Information for Site Characterisation. Network of Research Infrastructures for European Seismology, Deliverable JRA4-D4

Foti S, Hollender F, Garofalo F, Albarello D, Asten M, Bard P-Y, Comina C, Cornou C, Cox B, Di Giulio G, Forbriger T, Hayashi K, Lunedei E, Martin A, Mercerat D, Ohrnberger M, Poggi V, Renalier F, Sicilia D, Socco V (2018) Guidelines for the good practice of surface wave analysis: a product of the InterPACIFIC project. B Earthq Eng 16(6):2367–2420. https://doi.org/10.1007/s10518-017-0206-7

Gouveia F, da Fonseca AV, Gomes RC, Teves-Costa P (2018) Deeper $V_S$ profile constraining the dispersion curve with the ellipticity curve: A case study in Lower Tagus Valley, Portugal. Soil Dyn Earthq Eng 109:188–198. https://doi.org/10.1016/j.soildyn.2018.03.010

Grelle G, Guadagno FM (2009) Seismic refraction methodology for groundwater level determination: "Water seismic index". J Appl Geophys 68:301–320. https://doi.org/10.1016/j.jappgeo.2009.02.001

Grünthal G, GSHAP Region 3 working group (1999a) Seismic hazard assessment for Central, North and Northwest Europe: GSHAP Region 3. Ann Geophys-Italy 42(6):999–1101. https://doi.org/10.4401/ag-3783

Grünthal G, Bosse C, Sellami S, Mayer-Rosa D, Giardini D (1999b) Compilation of the GSHAP regional seismic hazard for Europe, Africa and the Middle East. Ann Geophys-Italy 42(6):1215–1223. https://doi.org/10.4401/ag-3782

Gröndal GO, Larsen G, Elefsen S (2005) Stærðir forsögulegra hamfaraflóða í Markarfljóti – mæling á farvegum neðan Einhyrningsflata. In: Guðmundsson MT, Gylfason ÁG (eds), Hættumat vegna eldgosa

og hlaupa frá vestanverðum Mýrdalsjökli og Eyjafjallajökli. Reykjavik: Ríkislögreglustjórinn and Háskólaútgáfan, pp 99–104 [in Icelandic]

Halldorsson B, Olivera CI, Rahpeyma S, Ólafsson S, Green RA, Snæbjörnsson JTh (2016) On the HVSR estimation at Icelandic strong-motion stations. Proceedings of the 17th Nordic Geotechnical Meeting, Reykjavík, Iceland, pp 1243–1252

Hallo M, Imperatori W, Panzera F, Fäh D (2021) Joint multizonal transdimensional Bayesian inversion of surface wave dispersion and ellipticity curves for local near-surface imaging. Geophys J Int 226:627–659. https://doi.org/10.1093/gji/ggab116

Hasan M, Shang Y (2022) Hard-rock investigation using a non-invasive geophysical approach. J Appl Geophys 206:104808. https://doi.org/10.1016/j.jappgeo.2022.104808

Haskell NA (1953) The dispersion of surface waves on multilayered media. B Seismol Soc Am 43(1):17–34. https://doi.org/10.1785/BSSA0430010017

Herrmann RB (1994) Computer programs in seismology, vol. IV. St. Louis, MO: St. Louis University

Hobiger M, Bard PY, Cornou C, Le Bihan N (2009) Single station determination of Rayleigh wave ellipticity by using the random decrement technique (RayDec). Geophys Res Lett 36:L14303. https://doi.org/10.1029/2009GL038863

Hobiger M, Le Bihan N, Cornou C, Bard PY (2012) Multicomponent Signal Processing for Rayleigh Wave Ellipticity Estimation: Application to Seismic Hazard Assessment. IEEE Signal Proc Mag 29(3):29–39. https://doi.org/10.1109/MSP.2012.2184969

Hobiger M, Cornou C, Wathelet M, Di Giulio G, Knapmeyer-Endrun B, Renalier F, Bard PY, Savvaidis A, Hailemikael S, Le Bihan N, Ohrnberger M, Theodoulidis N (2013) Ground structure imaging by inversions of Rayleigh wave ellipticity: sensitivity analysis and application to European strong-motion sites. Geophys J Int 192(1):207–229. https://doi.org/10.1093/gji/ggs005

Hunter JA, Crow HL, Dietiker B, Pugin AJM, Brewer K, Cartwright T (2020) A compilation of microtremor horizontal-to-vertical spectral ratios (HVSRs) and borehole shear-wave velocities of unconsolidated sediments in south-central Ontario. Geological Survey of Canada, Open File 8725. https://doi.org/10.4095/326133

Icelandic Road Administration (1986) Ölfusárós byggingarteikningar [structural drawings of Ölfusá Bridge, in Icelandic]

Ivanov J, Miller RD, Lacombe P, Johnson CD, Lane Jr. JW (2006) Delineating a shallow fault zone and dipping bedrock strata using multichannal analysis of surface waves with a land streamer. Geophysics 71(5):A39–A42. https://doi.org/10.1190/1.2227521

Jónasson K, Bessason B, Helgadóttir Á, Einarsson P, Gudmundsson GB, Brandsdóttir B, Vogfjord KS, Jónsdóttir K (2021) A harmonised instrumental earthquake catalogue for Iceland and the northern Mid-Atlantic Ridge. Nat Hazards Earth Syst Sci 21(7):2197–2214. https://doi.org/10.5194/nhess-21-2197-2021

Jonsson MH, Bessason B, Haflidason E (2010) Earthquake response of a base-isolated bridge subjected to strong near-fault ground motion. Soil Dyn Earthq Eng 30:447–455. https://doi.org/10.1016/j.soildyn.2010.01.001

Knopoff L (1964) A matrix method for elastic wave problems. B Seismol Soc Am 54(1):431–438. https://doi.org/10.1785/BSSA0540010431

Konno K, Ohmachi T (1998) Ground-motion characteristics estimated from spectral ratio between horizontal and vertical components of microtremor. B Seismol Soc Am 88(1):228–241

Kramer SL (2014) Geotechnical earthquake engineering. Harlow, England: Pearson Education Limited

Lai CG, Foti S, Rix GJ (2005) Propagation of data uncertainty in surface wave inversion. J Environ Eng Geoph 10(2):219–228. https://doi.org/10.2113/JEEG10.2.219

Larsen G, Smith K, Newton A, Knudsen Ó (2005) Jökulhlaup til vesturs frá Mýrdalsjökli: Ummerki um forsöguleg hlaup niður Markarfljót. In: Guðmundsson MT, Gylfason ÁG (eds) Hættumat vegna eldgosa og hlaupa frá vestanverðum Mýrdalsjökli og Eyjafjallajökli. Reykjavik: Ríkislögreglustjórinn and Háskólaútgáfan, pp 75–98 [in Icelandic]

Larsen G, Guðmundsson MT, Sigmundsson F, Höskuldsson Á, Jakobsdóttir SS, Oddson B, Magnússon E, Högnadóttir Th, Thórðarson Th, Björnsson H (2013) Eruption in Eyjafjallajökull 2010. In: Sólnes J, Sigmundsson F, Bessason B (eds) Natural Hazard in Iceland: Volcanic Eruptions and Earthquakes. Reykjavik: University of Iceland Press and Iceland Catastrophe Insurance, pp 299–311 [in Icelandic]

Nakamura Y (1989) A method for dynamic characteristics estimation of subsurface using microtremor on the ground surface. Quarterly Report of RTRI 30(1):25–33

Michel C, Edwards B, Poggi V, Burjánek J, Roten D, Cauzzi C, Fäh D (2014) Assessment of site effects in Alpine regions through systematic site characterization of seismic stations. Bull Seismol Soc Am 104(6): 2809–2826. https://doi.org/10.1785/0120140097

Molnar S, Sirohey A, Assaf J, Bard PY, Castellaro S, Cornou C, Cox B, Guillier B, Hassani B, Kawase H, Matsushima S, Sánchez-Sesma FJ, Yong A (2022) A review of the microtremor horizontal-to-vertical spectral ratio (MHVSR) method. J Seismol 26:653–685. https://doi.org/10.1007/s10950-021-10062-9

Olafsdottir EA (2019) Multichannel Analysis of Surface Waves for Soil Site Characterization. Dissertation, University of Iceland

Olafsdottir EA, Bessason B, and Erlingsson S (2018a) Combination of dispersion curves from MASW measurements. Soil Dyn Earthq Eng 113:473–487. https://doi.org/10.1016/j.soildyn.2018.05.025

Olafsdottir EA, Erlingsson S, Bessason B (2018b) Tool for analysis of multichannel analysis of surface waves (MASW) field data and evaluation of shear wave velocity profiles of soils. Can Geotech J 55(2):217–233. https://doi.org/10.1139/cgj-2016-0302

Olafsdottir EA, Bessason B, Erlingsson S (2019) Application of MASW in the South Iceland Seismic Zone. In: Rupakhey R, Olafsson S, Bessason B (eds) Proceedings of the International Conference on Earthquake Engineering and Structural Dynamics. Springer, Cham, pp 53–66. https://doi.org/10.1007/978-3-319-78187-7_5

Olafsdottir EA, Bessason B, Erlingsson S (2022) Non-invasive active- and passive-source stiffness characterization at a loose sand site. Proceedings of the 20th International Conference on Soil Mechanics and Geotechnical Engineering, Sidney, Australia, pp 501–506

Olivera CI, Halldorsson B, Ólafsson S, Green RA, Sigbjörnsson R (2014) A first look at site effects at Icelandic strong-motion stations using microseismic data. Proceedings of the 2nd European Conference on Earthquake Engineering and Seismology, Istanbul, Turkey, pp 1483–1490

Paolucci R, Aimar M, Ciancimino A, Dotti M, Foti S, Lanzano G, Mattevi P, Pacor F, Vanini M (2021) Checking the site categorization criteria and amplification factors of the 2021 draft of Eurocode 8 Part 1–1. B Earthq Eng 19:4199–4234. https://doi.org/10.1007/s10518-021-01118-9

Park CB, Miller RD, Xia J (1998) Imaging dispersion curves of surface waves on multi-channel record. SEG Technical Program Expanded Abstracts of the Society of Exploration Geophysicists (SEG) International Exposition and 68th Annual Meeting, New Orleans, LA, pp 1377–1380. https://doi.org/10.1190/1.1820161

Park CB, Miller RD, Xia J (1999) Multichannel analysis of surface waves. Geophysics 64(3):800–808. https://doi.org/10.1190/1.1444590

Parolai S, Picozzi M, Richwalski SM, Milkereit C (2005) Joint inversion of phase velocity dispersion and H/V ratio curves from seismic noise recordings using a genetic algorithm, considering higher modes. Geophys Res Lett 32(1):L01303. https://doi.org/10.1029/2004GL021115

Passeri F, Comina C, Foti S, Socco LV (2021) The Polito Surface Wave flat-file Database (PSWD): statistical properties of test results and some inter-method comparisons. B Earthq Eng 19:2343–2370. https://doi.org/10.1007/s10518-021-01069-1

Pétursson GS, van Rijn L, Pálmarsson SÓ, Myer EM, Ragnarsson E (2020) Landeyjahöfn harbour preliminary independent evaluation. Data review and assessment of harbour utilization. Report no. 20.07 / 2020-L-I. Ministry of Transport and Local Government, Reykjavik

Picozzi M, Parolai S, Richwalski SM (2005) Joint inversion of H/V ratios and dispersion curves from seismic noise: Estimating the S-wave velocity of bedrock. Geophys Res Lett 32(11):L11308. https://doi.org/10.1029/2005GL022878

Rahpeyma S, Halldorsson B, Olivera C, Green RA, Jónsson S (2016) Detailed site effect estimation in the presence of strong velocity reversals within a small-aperture strong-motion array in Iceland. Soil Dyn Earthq Eng 89:136–151. https://doi.org/10.1016/j.soildyn.2016.07.001

Roy N, Jakka RS (2018) Effect of data uncertainty and inversion non-uniqueness of surface wave tests on $V_{S,30}$ estimation. Soil Dyn Earthq Eng 113:87–100. https://doi.org/10.1016/j.soildyn.2018.02.030

Sambridge M (1999) Geophysical inversion with a neighbourhood algorithm — I. Searching a parameter space. Geophys J Int 138(2):479–494. https://doi.org/10.1046/j.1365-246X.1999.00876.x

Sarjan AFN, Zulfakriza Z, Nugraha AD, Rosalia S, Wei S, Widiyantoro S, Cummins PR, Muzli M, Sahara DP, Puspito NT, Priyono A, Afif H (2021) Delineation of upper crustal structure beneath the Island of Lombok, Indonesia, using ambient seismic noise tomography. Front Earth Sci 9:560428. https://doi.org/10.3389/feart.2021.560428

Scherbaum F, Hinzen KG, Ohrnberger M (2003) Determination of shallow shear wave velocity profiles in the Cologne, Germany area using ambient vibrations. Geophys J Int 152(3):597–612. https://doi.org/10.1046/j.1365-246X.2003.01856.x

SESAME (2004) Guidelines for the Implementation of the H/V Spectral Ratio Technique on Ambient Vibrations: Measurements, Processing, and Interpretations. SESAME European research project. WP12 – Deliverable D23.12

Sharafeldin MS, Essa KS, Youssef MAS, Karsli H, Diab ZE, Sayıl N (2019) Shallow geophysical techniques to investigate the groundwater table at the Great Pyramids of Giza, Egypt. Geosci Instrum Method Data Syst 8:29–43. https://doi.org/10.5194/gi-8-29-2019

Sigbjörnsson R, Ólafsson S (2004) On the South Iceland earthquakes in June 2000: strong-motion effects and damage. Bollettino di Geofisica Teorica ed Applicata 45(3):131–152

Sigbjörnsson R, Snæbjörnsson·JTh, Higgins SM, Halldórsson B, Ólafsson S (2009) A note on the $M_w$6.3 earthquake in Iceland on 29 May 2008 at 15:45 UTC. B Earthq Eng 7:113–126. https://doi.org/10.1007/s10518-008-9087-0

Sigurðsson GÖ, Rupakhety R, Ólafsson S (2017) Site Response Evaluation in a Volcanic Area using H/V and 1 D wave Propagation Analysis. Proceedings of the 16th World Conference on Earthquake Engineering, Santiago, Chile. Paper no. 4495

Skúlason J, Bessason B, Rafnsson EÁ, Sigursteinsson H (2002) Liquefaction of sediments. Yearbook of the Association of Chartered Engineers in Iceland 14:250–258 [in Icelandic]

Steeples DW (2005) Shallow Seismic Methods. In: Rubin Y, Hubbard SS (eds) Hydrogeophysics. Water Science and Technology Library, vol 50. Dordrecht, the Netherlands: Springer, pp. 215–251. https://doi.org/10.1007/1-4020-3102-5_8

Sæmundsson K (1979) Outline of the geology of Iceland. Jökull 29:7–28

Thomson WT (1950) Transmission of elastic waves through a stratified solid medium. J Appl Phys 21:89–93. https://doi.org/10.1063/1.1699629

Viggosson G, Jónsdóttir I, Sigurðarson S, Bernódusson J (2005) A Ferry and Ferry Port on the Exposed South Coast of Iceland. A proposal for a practical solution for transport between Vestmannaeyjar and mainland Iceland. Proceedings of the Second International Coastal Symposium in Iceland, Höfn, Iceland

Vogfjörð K, Sigbjörnsson R, Snæbjörnsson JÞ, Halldórsson B, Sólnes J, Stefánsson R (2013) The South Iceland Earthquakes 2000 and 2008. In: Sólnes J, Sigmundsson F, Bessason B (eds.) Natural Hazard in Iceland: Volcanic Eruptions and Earthquakes. University of Iceland Press and Iceland Catastrophe Insurance, Reykjavik, pp 611–633 [in Icelandic]

Wang Z, Sun C Wu D (2022) Near-surface Site Characterization Based on Joint Iterative Analysis of First-arrival and Surface-wave Data. Surv Geophys. https://doi.org/10.1007/s10712-022-09747-8

Wathelet M (2005) Array Recordings of Ambient Vibrations: Surface-Wave Inversion. Dissertation, Liége University

Wathelet M (2008) An improved neighborhood algorithm: parameter conditions and dynamic scaling. Geophys Res Lett 35:L09301. https://doi.org/10.1029/2008GL033256

Wathelet M, Jongmans D, Ohrnberger M (2004) Surface wave inversion using a direct search algorithm and its application to ambient vibration measurements. Near Surf Geophys 2(4):211–221 https://doi.org/10.3997/1873-0604.2004018

Wathelet M, Chatelain JL, Cornou C, Di Giulio G, Guillier B, Ohrnberger M, Savvaidis, A (2020) Geopsy: A User-Friendly Open-Source Tool Set for Ambient Vibration Processing. Seismol Res Lett 91(3):1878–1889. https://doi.org/10.1785/0220190360